Atmos. Chem. Phys., 12, 9719–9738, 2012
www.atmos-chem-phys.net/12/9719/2012/
doi:10.5194/acp-12-9719-2012

Atmospheric Chemistry and Physics

Columnar aerosol properties from sun-and-star photometry: statistical comparisons and day-to-night dynamic

D. Pérez-Ramírez[1,2,3], **H. Lyamani**[1,2], **F. J. Olmo**[1,2], **D. N. Whiteman**[3], **and L. Alados-Arboledas**[1,2]

[1]Centro Andaluz de Medio Ambiente (CEAMA), Universidad de Granada, Junta de Andalucía, Av. del Mediterráneo s/n, 18006-Granada, Spain
[2]Departamento de Física Aplicada, Universidad de Granada, Campus de Fuentenueva s/n, 18071-Granada, Spain
[3]Mesoscale Atmospheric Processes Laboratory, NASA Goddard Space Flight Center, 20771, Greenbelt-Maryland, USA

Correspondence to: D. Pérez-Ramírez (daniel.perezramirez@nasa.gov)

Received: 29 March 2012 – Published in Atmos. Chem. Phys. Discuss.: 9 May 2012
Revised: 10 September 2012 – Accepted: 20 September 2012 – Published: 25 October 2012

Abstract. This work presents the first analysis of long-term correlative day-to-night columnar aerosol optical properties. The aim is to better understand columnar aerosol dynamic from ground-based observations, which are poorly studied until now. To this end we have used a combination of sun-and-star photometry measurements acquired in the city of Granada (37.16° N, 3.60° W, 680 m a.s.l.; South-East of Spain) from 2007 to 2010. For the whole study period, mean aerosol optical depth (AOD) around 440 nm (±standard deviation) is 0.18 ± 0.10 and 0.19 ± 0.11 for daytime and nighttime, respectively, while the mean Angström exponent (α) is 1.0 ± 0.4 and 0.9 ± 0.4 for daytime and nighttime. The ANOVA statistical tests reveal that there are no significant differences between AOD and α obtained at daytime and those at nighttime. Additionally, the mean daytime values of AOD and α obtained during this study period are coherent with the values obtained in the surrounding AERONET stations. On the other hand, AOD around 440 nm present evident seasonal patterns characterised by large values in summer (mean value of 0.20 ± 0.10 both at daytime and nighttime) and low values in winter (mean value of 0.15 ± 0.09 at daytime and 0.17 ± 0.10 at nighttime). The Angström exponents also present seasonal patterns, but with low values in summer (mean values of 0.8 ± 0.4 and 0.9 ± 0.4 at day- and night-time) and relatively large values in winter (mean values of 1.2 ± 0.4 and 1.0 ± 0.3 at daytime and nighttime). These seasonal patterns are explained by the differences in the meteorological conditions and by the differences in the strength of the aerosol sources. To take more insight about the changes in aerosol particles between day and night, the spectral differences of the Angström exponent as function of the Angström exponent are also studied. These analyses reveal increases of the fine mode radius and of the fine mode contribution to AOD during nighttime, being more remarkable in the summer seasons. These variations are explained by the changes of the local aerosol sources and by the meteorological conditions between daytime and nighttime, as well as aerosol aging processes. Case studies during summer and winter for different aerosol loads and types are also presented to clearly illustrate these findings.

1 Introduction

Atmospheric aerosol is noted by the Fourth Intergovernmental Panel for Climate Change (IPCC 2007) as a key component on the climate (Forster et al., 2007). Atmospheric aerosol particles directly affect Earth's radiation budget by scattering short-wavelengths radiation and absorbing shortwave and longwave radiation (e.g., Haywood and Shine, 1997; Forster et al., 2007). Furthermore, atmospheric aerosol particles can act as cloud condensation nuclei and, thus, they can modify cloud droplet size and cloud albedo (Forster et al., 2007). In addition, they have effects on air quality and, thus, on the human health (e.g., Pope et al., 2002; Brunekreef and Forsberg, 2005; Miller et al., 2007). The IPCC 2007 also reported that due to the lack of adequate information on aerosol temporal and spatial variability the uncertainties associated with each aerosol effect are much larger than those associated with greenhouse gases. Therefore, it is really

important to measure and characterise the aerosol properties in different sites for better understanding the aerosol impact at least at regional scale.

Research on the atmospheric effects of the aerosol particles has become a top priority. In this sense, several satellite programmes have been developed to study long-term spectral aerosol optical depth (AOD) on a global scale (e.g., Kaufman et al., 1997, 2002; Kahn et al., 2005; Remer et al., 2005). However, satellite measurements present low temporal resolution. Surface-based passive measurements allow the study of columnar aerosol properties, and the global network AERONET (Holben et al., 1998) has been developed. But all these instrumentations acquire measurements at daytime. Currently, Raman lidar systems allow retrieving vertical profiles of aerosol optical properties at nighttime, but the high cost of this technique make these measurements sparse in time (Bösenberg et al., 2001; Pappalardo et al., 2009). Other simpler configurations, such as elastic lidar systems, can also acquire nighttime measurements, but they need constraints as the extinction-to-backscatter ratio (Sassano et al., 1989; Welton et al., 2001).

Until now, the knowledge of columnar aerosol properties at nighttime is quite limited due to the absence of continuous measurements. Although the role of columnar aerosol at nighttime in radiative forcing is weak because only small aerosol absorption is expected in the thermal infrared, the knowledge of nighttime columnar aerosol properties is very important to evaluate aerosol dynamic. These studies will allow us to have a whole picture of the daily behaviour of the atmospheric aerosol, covering the different stages in the evolution of the planetary boundary layer and pre-convection and pre-photochemistry processes that affect the atmospheric aerosol. The knowledge of AOD at nighttime will also contribute to aerosol transport and chemistry models validation efforts, being important within the air-quality schemes. In addition, the AOD at nighttime can be also used as constraints for correlative lidar measurements (e.g., Alados-Arboledas et al., 2011), both for ground-based and space-borne missions. Therefore, research studies about columnar aerosol properties at nighttime are calling for and currently some research groups are working with ground-based irradiance measurements from stars (e.g., Herber et al., 2002; Perez-Ramirez et al., 2008a; Baibakov et al., 2009) or from the moon (e.g., Esposito et al., 1998; Herber et al., 2002; Berkoff et al., 2011) to obtain AOD at nighttime.

First attempts in star-photometry were made by Leiterer et al. (1995) who developed an instrument based on a photodetector as measurement device, acquiring very valuable measurements during 10 days in April 1994 at the Lindenberg observatory (52.14° N; 14.12° E; Germany). This design was also used by Herber et al. (2002) to acquire measurements during the Arctic winter from 1996 to 1999 at the Koldeway station in Ny-Ålesund (78.95° N; 11.93° E; Norway). However, these last studies did not deal with correlative day-to-night measurements due to the characteristics of the place. Moreover, evaluations of daytime and nighttime differences in particle sizes (types) were not performed.

To address the problem of the lack of continuous measurements of spectral AOD at nighttime, this work uses the measurements acquired by the star photometer EXCALIBUR based on a CCD camera as detector device (Perez-Ramirez et al., 2008a, b). This instrument, together with a sun photometer CIMEL, operates in the Andalusian Center for Environmental Research in the city of Granada (37.16° N, 3.60° W, 680 m a.s.l.; South-East of Spain). The star photometer EXCALIBUR is also a versatile instrument because it is able to obtain precipitable water vapour (Perez-Ramirez et al., 2012a) and is also used to estimate the sky quality in Astronomical Centers (Sanchez et al., 2007).

Moreover, atmospheric aerosol particles are constantly affected by physical and chemical processes in the atmosphere that induce changes in the optical and radiative properties of these particles. The spectral dependence of AOD is related to the sizes (types) of the predominant particles. Thus, using sun/star photometry, the possible changes in aerosol particle sizes (types) can be analysed by means of studying the spectral dependence of AOD (e.g., O'Neill et al., 2001, 2003; Schuster, 2006; Gobbi et al., 2007) or by studying aerosol size distributions retrieved by inversion methods using sky radiance measurements (e.g., Dubovik and King, 2000; Dubovik et al., 2006; Olmo et al., 2006, 2008). In this work, in order to study the possible change in the aerosol particle sizes between daytime and nighttime, and due to the lack of sky radiance measurements by star photometry, we use the simple graphical method proposed by Gobbi et al. (2007).

The scope of this work is to study day-to-night columnar aerosol properties which, to our knowledge, have not been already done. To this end, we use consecutive day-to-night sun/star photometry measurements acquired between 2007 and 2010 in the city of Granada (Spain). The instruments used and the experimental site are described in Sect. 2. The descriptions of the methodologies are in Sect. 3. Later, in Sect. 4 we present the main results, with an in depth analysis of intra-annual and seasonal evolutions of columnar aerosol properties, as well as the spectral analysis of the Angström exponent, both at daytime and nighttime. We also present two case studies related to the air-masses origin in order to show day-to-night columnar aerosol dynamic. Concluding remarks are given in Sect. 5.

2 Instrumentation and experimental site

Column-integrated characterisation of the atmospheric aerosol at daytime has been performed by means of a sun-photometer CIMEL CE-318-4 (Cimel Electronique, France), while at nighttime a star-photometer EXCALIBUR (Astronómica S.L.) has been used. The CIMEL CE-318-4 makes solar extinction measurements with a 1.2° full field-of-view

at 340, 380, 440, 670, 870, 940 and 1020 nm. The full-width at half-maximum (FWHM) of the interference filters are 2 nm at 340 nm, 4 nm at 380 nm and 10 nm for the other wavelengths. More details about the CIMEL CE-318-4 can be found in e.g., Holben et al. (1998); Alados-Arboledas et al. (2008). On the other hand, for nighttime the star photometer EXCALIBUR acquires direct star irradiance measurements at 380, 436, 500, 670, 880, 940 and 1020 nm (nominal wavelengths). The FWHM range between 7.7 and 11.2 nm for the different filters. EXCALIBUR star photometer presents the difference to those previously developed by Leiter et al. (1995) that uses a CCD camera as detector device. Further details about this instrument can be found in Perez-Ramirez et al. (2008a, b). Both instruments operated in the Andalusian Center for Environmental Research (CEAMA) located in the city of Granada (37.16° N, 3.60° W, 680 m a.s.l.; South-East of Spain). Granada is a non-industrialised and medium-sized city, with a municipal population around 250 000 inhabitants and twice including its metropolitan area. The city is situated in a natural basin surrounded by mountains, with the highest hills over 3000 m a.s.l. located at the Southeast of the basin. The Mediterranean-Continental climate conditions prevailing at this site are responsible for large seasonal temperature differences, providing mild winters and hot summers. On the other hand, most of the rainfall is registered in spring–winter. The summers are usually very dry, with very few rainfall events. For the past 50 yr, according to Spanish Meteorological Agency (AEMET; http://www.aemet.es), the mean annual rainfall in this area is 370 mm. The relative humidity (RH) is larger in winter (with average values of 60 % and 70 % for daytime and nighttime, respectively) than in summer (38 % and 49 % for daytime and nighttime, respectively). Finally, the RH shows a clear diurnal cycle in all the seasons with the largest values at night and the lowest values at noon.

Due to its location in the Iberian Peninsula, the study area is usually affected by air-masses with different origins. By one hand, air-masses with origin in the Sahara desert (North Africa) are usually associated with large amounts of mineral dust particles (e.g., Lyamani et al., 2005, 2006a, b; Guerrero-Rascado et al., 2009; Valenzuela et al., 2012a, b). These air-masses are more frequent during the summer season (Valenzuela et al., 2012b). On the other hand, the air-masses coming from Europe or from the Mediterranean basin can transport large loads of anthropogenic particles to the study area (e.g., Lyamani et al., 2006a, b). Atlantic air-masses affecting the study area are usually associated with low aerosol loads (e.g., Lyamani et al., 2010), being more frequent in the winter season. Furthermore, the main local anthropogenic source of aerosol particles is traffic, and also domestic heating (based on fuel oil combustion) in winter (e.g., Lyamani et al., 2008, 2010, 2011; Titos et al., 2012).

3 Methodology

Attenuation of sun or star irradiance through the Earth's atmosphere follows the Beer-Bouger-Lambert law that is given by (for an average Sun/star-Earth distance):

$$V(\lambda) = V_0(\lambda) \exp(-m_r \delta_{atm}(\lambda)) \quad (1)$$

where $V(\lambda)$ is the signal measured by the photometer, $V_0(\lambda)$ is the extraterrestrial signal (what is known as calibration constant), m_r is the optical relative air mass and $\delta_{atm}(\lambda)$ is the total atmospheric optical depth. The calibration of the star photometer EXCALIBUR was performed at the high mountain site of Calar Alto (37.2° N, 2.5° W, 2168 m a.s.l.), once a year (Perez-Ramirez et al., 2011). Calibration of sun photometer Cimel was performed twice a year in "Ahí de Cara" (37.1° N, 3.4° W, 2100 m a.s.l.) (Alados-Arboledas et al., 2008) following the same calibration procedures of the AERONET network (Holben et al., 1998). Using equation 1 and sun/star photometer measurements, the aerosol optical depth (AOD(λ)) at the selected spectral channels have been computed following the methods described in the works of Alados-Arboledas et al. (2003, 2008) and Perez-Ramirez et al. (2008a), for sun- and star-photometers, respectively. Uncertainties in AOD(λ) for the star-photometer EXCALIBUR are 0.02 for $\lambda < 800$ nm and 0.01 for $\lambda > 800$ nm (Perez-Ramirez et al., 2011), and for sun-photometer CIMEL are 0.02 for $\lambda < 400$ nm and 0.01 for $\lambda > 400$ nm (Holben et al., 1998).

From the Angström turbidity formula $\mathrm{AOD}(\lambda) = \beta\lambda^{-\alpha}$, least-squares fits (in a log-log scale) were applied to determine the coefficients α and β. The β parameter is related to particle concentration and represents the aerosol optical depth at 1 µm. In the solar spectrum, the Angström exponent α characterises the spectral features of aerosol particles and is related to the size of the particles; $\alpha > 1.5$ are mainly determined by the fine mode (submicron aerosol particles), while $\alpha < 0.5$ are largely determined by the coarse mode (e.g., Dubovik et al., 2002; Gobbi et al., 2007). In this work, the Angström exponent, α(436–880 nm), obtained at nighttime is computed from AOD at 436, 667, 880 nm and the Angström exponent, α(440–870 nm), obtained at daytime is calculated from AOD at 440, 670 and 870 nm.

Several authors have discussed how the spectral curvature of the Angström exponent α can provide further information about the aerosol size distribution (e.g., Eck et al., 1999; O'Neill et al., 2001, 2003; Schuster, 2006; Gobbi et al., 2007). In this work, we use the simple graphical method proposed by Gobbi et al. (2007). In this method, for a bimodal size distribution with different fine (r_f) and coarse (r_c) modal radius and fixed widths of fine and coarse modes of $\sigma_f = 1.5$ µm and $\sigma_c = 1.8$ µm, respectively, the difference $\delta\alpha = \alpha(440\text{–}670\,\mathrm{nm}) - \alpha(670\text{–}870\,\mathrm{nm})$ was computed and represented versus α(440–870 nm). This computation was also made taking into account different contributions of the fine mode to AOD at 670 nm (η). The computations were

done using the Mie theory with a fixed aerosol refractive index $m = 1.4–0.001i$ (Gobbi et al., 2007). Moreover, this method assumes that the particles are spherical, which has no significant impact on the results (Gobbi et al., 2007). It is important to note that due to the large uncertainties in the Angström exponent for low AOD(λ), this method is only applicable for AOD(670 nm) > 0.15 (Gobbi et al., 2007).

Although sun- and star-photometers have filters centred at the same wavelengths, there are small differences in those around 440 and 880 nm. We have studied the effects of these small differences by evaluating $\mathrm{AOD}(\lambda) = \beta\lambda^{-\alpha}$. The parameter α was set at 0.2, 0.5, 0.75, 1.0, 1.25, 1.5, 1.75, 2.0 and 2.5 while the parameter β was set at 0.05, 0.1, 0.2, 0.3, 0.4, 0.5, 0.6, 0.7, 0.8, 0.9, 1.0, 1.25, 1.5 and 2.0. From these computed AOD(λ), the Angström parameter α(440–870 nm), α(436–880 nm), α(440–670 nm), α(436–670 nm), α(670–870 nm) and α(670–880 nm) were after computed, reproducing each one same initial α values. To take more insight of the effect of these slight differences in filters between both instruments, we also evaluated the relative differences (AOD(440) – AOD(436))/AOD(440) and (AOD(870) – AOD(880))/AOD(870). No differences were found out for fixed values of α and variable β. However, there were slight differences varying α and being β fixed: for $\alpha < 1$ we obtained that both relative differences are lower than 1 %, while for $\alpha > 1$ they are lower than 2 %. Taking into account that $\Delta\alpha \sim (\Delta\mathrm{AOD}_1/\mathrm{AOD}_1 + \Delta\mathrm{AOD}_2/\mathrm{AOD}_2)$ (where the subscripts 1 and 2 refer to the different wavelength used in the computations), we obtained $\Delta\alpha$(440–870 nm) < 2 %, $\Delta\alpha$(440–670 nm) < 1 %, $\Delta\alpha$(670–880 nm) < 1 % and $\Delta\delta\alpha < 2$ % for $\alpha < 1$, while $\Delta\alpha$(440–870 nm) < 4 %, $\Delta\alpha$(440–670 nm) < 2 %, $\Delta\alpha$(670–880 nm) < 2 % and $\Delta\delta\alpha < 4$ % for $\alpha > 1$. These uncertainties are lower than those associated with the sun- and star-photometers used in this work.

Finally, five-day backward-trajectories of the air-masses affecting the study area are calculated by the HYSPLIT-4 model (Draxler and Rolph, 2003). The meteorological data used to run the model are 6-hourly GDAS (Global Data Assimilation System, ftp://www.arl.noaa.gov/pub/archives/gdas1/). The HYSPLIT model has been run twice a day at 00:00 and 12:00 UTC at 1500 m a.g.l.; this altitude was selected as representative of the whole atmospheric column (e.g., Toledano et al., 2009). To classify the air-masses that affected the study area we follow the classification scheme developed by Toledano et al. (2009). This method is based on the residence time of the trajectory within geographic sectors. We defined five major air-mass sectors: North Atlantic Ocean (maritime-polar), South Atlantic Ocean (maritime-tropical), European Continent and Iberian Peninsula (continental), Mediterranean Sea (Eastern), North Africa (Southern) and the Local one.

4 Results

The data used in this work were acquired from 2007 to 2010. Aerosol optical depths obtained by the sun-photometer were cloud-screened using the algorithm proposed by Smirnov et al. (2000) (used in AERONET network). For nighttime, the star photometer cloud-free data were obtained applying the algorithm proposed by Perez-Ramirez et al. (2012b). Additionally, the days and nights that present less than 2 h of measurements were eliminated from the database. Monthly values with less than 8 days/nights of measurements were also eliminated.

4.1 Temporal evolution of columnar aerosol optical depth and Angström exponent

Figure 1 shows the temporal evolutions of daytime mean values of AOD(440 nm) and nighttime mean values of AOD(436 nm) acquired at Granada during the study period. Monthly values are also plotted. There are some gaps in both AOD(λ) data series which are due to instruments maintenance and calibration as well as to bad meteorological conditions.

From Fig. 1, both at daytime and nighttime, there are variations in AOD(λ) which are generally of random nature. However, these random variations are modulated by more regular longer period variations. Low values of AOD(λ) are more frequently found during the winter months, while large values are frequently obtained in summer months, both at daytime and nighttime.

Figure 2 shows the temporal evolutions of daytime mean values of α(440–870 nm) and nighttime mean values of α(436–880 nm). Monthly values are also plotted. As for AOD(λ), there is an important variability in the Angström exponent values between day-to-day and night-to-night. During the daytime, α(440–870 nm) shows large values in winter and low values in summer months. However, during the nighttime these seasonal differences are not so remarkable.

Table 1 presents a statistical summary of daytime and nighttime mean values of AOD(λ) and α for the whole study period; particularly the mean value, standard deviation (STD), median, maximum and minimum values, as well as the corresponding percentiles at 10, 25, 75 and 90 % (P10, P25, P75 and P90). ANOVA statistical tests were used to compare daytime and nighttime datasets. These tests are based on the analysis of variances. The null hypothesis indicates that day and night data series are not different. The ANOVA statistical tests reveal that at 95 % level the datasets of AOD(λ) and α obtained at daytime are statistically equal to those obtained at nighttime. During daytime, AOD(440 nm) ranges from 0.02 to 0.95 with a mean value of 0.18 ± 0.10, while α(440–870 nm) varies between 0.01 and 1.8 with a mean value of 1.0 ± 0.4. During nighttime, AOD(436 nm) varies from 0.02 to 0.68 with a mean value of 0.19 ± 0.11, while α(436–880 nm), varies from 0.1

Table 1. Daytime and nighttime spectral aerosol optical depth AOD(λ) and Angström exponent α statistics for the 4-year data series in the city of Granada; STD is the standard deviation; P10, P25, P75 and P90 are the corresponding percentiles at 10, 25, 75 and 90 %.

Parameter	Aerosol Optical Depth (AOD) at different wavelenghts (nm)										Angström exponent	
Wavelenght (nm)	380	380	440	436	670	670	870	880	1020	1020	α(440–870)	α(436–880)
Time period	Day	Night	Day	Night	Day	Night	Day	Night	Day	Night	Day	Night
Mean	0.21	0.21	0.18	0.19	0.12	0.13	0.10	0.10	0.09	0.09	1.0	0.9
STD	0.11	0.13	0.10	0.11	0.08	0.09	0.08	0.08	0.08	0.07	0.4	0.4
P25	0.14	0.13	0.11	0.11	0.07	0.07	0.05	0.05	0.04	0.05	0.6	0.7
P75	0.26	0.27	0.22	0.24	0.14	0.16	0.12	0.13	0.10	0.11	1.3	1.2
P10	0.10	0.09	0.08	0.07	0.05	0.05	0.04	0.03	0.03	0.03	0.4	0.4
P90	0.34	0.38	0.29	0.32	0.22	0.24	0.20	0.19	0.20	0.17	1.5	1.4
Minimum	0.03	0.02	0.02	0.02	0.01	0.02	0.01	0.01	0.01	0.01	0.01	0.1
Maximum	1.07	0.90	0.95	0.68	0.94	0.63	0.91	0.62	0.90	0.59	1.8	2.1
Median	0.19	0.19	0.16	0.17	0.10	0.10	0.08	0.08	0.07	0.07	1.0	1.0

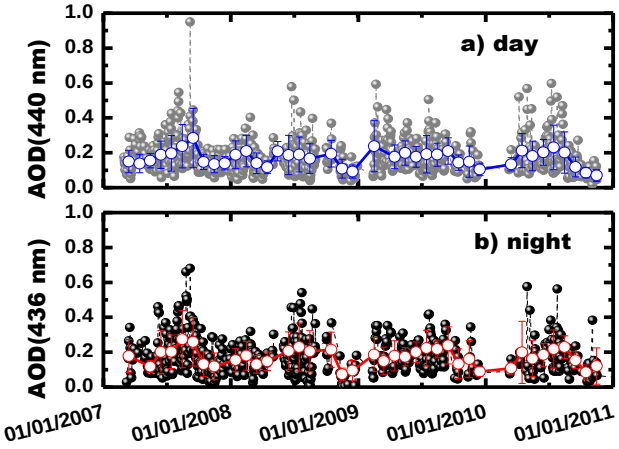

Fig. 1. (a) Temporal evolutions of daytime aerosol optical depth at 440 nm and **(b)** nighttime aerosol optical depth at 436 nm. Fully circles linked by dash lines corresponds to day/night mean values, while open circles linked by solid lines represents monthly day/night values and their standard deviations. All the data were acquired at Granada from 2007 to 2010.

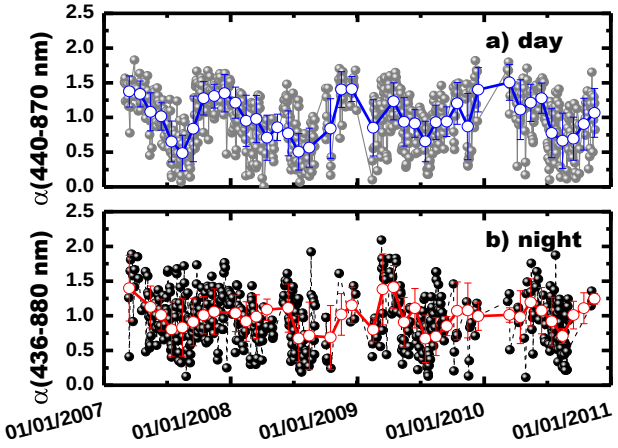

Fig. 2. (a) Temporal evolutions of daytime Angstrom exponent α(440–870 nm) and **(b)** nighttime Angstrom exponent α(436–880 nm). Fully circles linked by dash lines corresponds to day/night mean values, while open circles linked by solid lines represents monthly day/night values and their standard deviations. All the data were acquired at Granada from 2007 to 2010.

up to 2.1 with a mean value of 0.9 ± 0.4. Thus, there are no statistical significant differences in the sets of daytime and nighttime data of AOD(λ) and α.

The standard deviations and percentiles of AOD(λ) and α are large, both at daytime and nighttime, indicating the large variability of the atmospheric aerosol loads and types, and associated with the variability in the synoptic conditions. In fact, as mentioned before, the different air-masses affecting the study area are responsible of aerosol variability (e.g., Atlantic air-masses are very clean while North African air-masses can transport large loads of mineral dust; Continental and Mediterranean air-masses usually transport anthropogenic particles). Another factor that can explain the large variability is the changeable meteorological conditions. Rainfall events favour the aerosol wet deposition, leading to the reduction of the aerosol load. Additionally, very high values of AOD(λ), both at daytime and nighttime, can be also associated with extreme events such as pollution or biomass burning (e.g., Alados-Arboledas et al., 2011).

For the whole study period, Fig. 3 shows the frequency distributions of AOD(440 nm) and α(440–870 nm) obtained at daytime, and AOD(436 nm) and α(436–880 nm) obtained at nighttime. Both AOD(λ) frequency distributions are unimodal with strong skewness at low values of AOD(λ). The AOD(λ) modal value is 0.13 both at daytime and nighttime. On the other hand, the Angström exponent shows bimodal distributions both at daytime and nighttime. The first mode is centred at 0.55 and 0.45 with 6 % and 7 % frequencies of

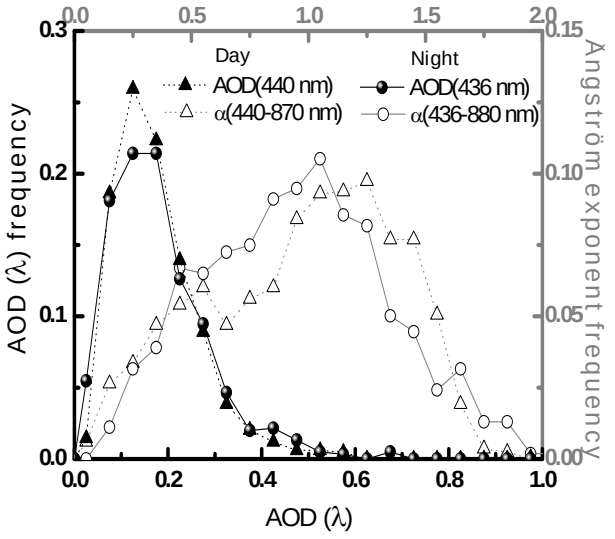

Fig. 3. Frequency histograms of AOD(440 nm) and α(440–870 nm) obtained at daytime and of AOD(436 nm) and α(436–880 nm) obtained at nighttime for the period 2007–2010.

occurrence at daytime and nighttime, respectively, which reflects the contribution of large particles associated with long-range transport of dust particles and with local re-suspended soil dust. The second mode is located at 1.25 and 1.05 with approximately 10 % frequencies of occurrence at daytime and nighttime, respectively, and evidences cases associated with a mixture of fine (mainly from anthropogenic origin) and coarse particles.

However, analysing only α values does not provide clear information about the changes of fine/coarse mode to the aerosol load. To take more insight about the day-to-night changes of α, we use the simple graphical method proposed by Gobbi et al. (2007). Figure 4 shows both daytime and nighttime $\delta\alpha$ versus α. The data presented in Fig. 4 correspond to daily or nightly mean values. The data that fall out of the diagrams in the upper region can be explained because they have fine mode radius (r_f) lower than 0.05 µm, while those in the bottom region can be explained by the use of a fixed refractive index (Gobbi et al., 2007).

From Fig. 4 changes in the fine mode fraction and radius between daytime and nighttime are observed, with increases of η and r_f at nighttime. For AOD(670 nm) ranging between 0.15 and 0.3, at daytime most of the data present r_f values ranging from 0.10 to 0.15 µm, while the fine mode fraction (η) varies a lot with values up to 70 % (Fig. 4a). The variability of r_f and η, and also of α(440–870 nm) (from 0.07 to 1.63) indicate large variability in the aerosol types and sizes. At nighttime a clockwise rotation toward larger r_f (up to 0.3 µm) and η (up to 99 %) is observed. For other ranges of AOD(670 nm), α is lower than 0.7 both at nighttime and daytime, and the clockwise rotation at nighttime is observed as well. Changes in η can be associated with differences in the aerosol supplies either by natural or anthropogenic emissions, and must be studied detailed for every season (see Sect. 4.3). The increase of r_f at nighttime might be associated with aerosol aging (e.g., Reid et al., 1998, 1999; Dubovik et al., 2002; Eck et al., 2001, 2003a, b).

4.2 Inter-comparison with surrounding AERONET stations

For the study period, Table 2 shows the mean AOD(440 nm) and α(440–870 nm) values obtained at 14 AERONET stations located in the Iberian Peninsula, Western Mediterranean Basin, North West Africa and Canary Island. For small urban areas in the Iberian Peninsula like Evora, Cáceres and Palencia, lower values of AOD(440 nm) than in the city of Granada are obtained. The α(440–870 nm) values at Granada are lower than those at Cáceres and Palencia. Atlantic flow advections are much more frequent in the West than in the East of the Iberian Peninsula (e.g., Querol et al., 2009), and the low aerosol load associated with these air-masses can explain the low values of AOD(440 nm) at Evora, Cáceres and Palencia. Additionally, the larger impact of Saharan dust outbreaks over the South of Spain (e.g., Querol et al., 2009; Toledano et al., 2007a, 2009) with large aerosol loads and low values of the Angström exponent (e.g., Lyamani et al., 2006a, b; Toledano et al., 2007a; Cachorro et al., 2008; Valenzuela et al., 2012a, b) can also explain the results obtained at Granada. On the other hand, although El Arenosillo is a remote station, the AOD in this site is quite similar to that obtained in Granada. This can be explained by the effects of anthropogenic industrial emissions in the South-West of Spain and by the Saharan dust intrusions over this remote station (e.g., Toledano et al., 2007b; Prats et al., 2008; Córdoba-Jabanero et al., 2011; Bennouna et al., 2011). The stations of Valencia and Barcelona present larger values of AOD(440 nm) and α(440–870 nm) than those at the station of Granada. These two sites correspond to bigger cities in Spain with considerable levels of local anthropogenic emissions. These sites are also affected by Saharan dust intrusions, but with less frequency compared to that at the station of Granada because Barcelona and Valencia are further to the dust sources in North Africa (e.g., Rodriguez et al., 2001; Estelles et al., 2007; Querol et al., 2009).

In other sites in the Western Mediterranean like Avignon, Ispra, Rome, Toulon and Lecce, AOD(440 nm) and α(440–870 nm) are larger than those obtained in Granada and in other more polluted sites in the Iberian Peninsula such as Valencia and Barcelona. This is because these cities (Avignon, Ispra, Rome, Toulon and Lecce) are urban areas with high local anthropogenic emissions and quite affected by highly polluted air-masses from Europe (e.g., Pace et al., 2006; Santese et al., 2008; Mazzola et al., 2010). In addition, they are also affected by Saharan dust intrusions (e.g., Perrone et al., 2005; Santese et al., 2008; Meloni et al., 2007; Pavese et al., 2009). It is worth noting that the station of Blida is

Table 2. Mean values of aerosol optical depths at 440 nm and α(440–870 nm) obtained during the period 2007–2010 at 14 AERONET stations. A brief description of each AERONET site is also included. The stations are defined as Desert areas (D), Remote (R), Urban sites (U) and Costal areas (C).

AERONET site	Coordinates	Class	Dataset	AOD (440nm)	α(440–870)
Iberian Peninsula					
El Aeronosillo	37.1° N, 6.7° W, 0 m a.s.l.	R/C	963	0.17 ± 0.12	1.0 ± 0.4
Cáceres	39.5° N, 6.3° W, 347 m a.s.l.	U	792	0.14 ± 0.09	1.3 ± 0.4
Evora	38.6° N, 7.9° W, 293 m a.s.l.	U	1097	0.15 ± 0.12	1.1 ± 0.5
Palencia	42.0° N, 4.5° W, 750 m a.s.l.	U	788	0.14 ± 0.12	1.3 ± 0.5
Valencia	39.5° N, 0.4° W, 30 m a.s.l.	UC	916	0.21 ± 0.14	1.1 ± 0.4
Barcelona	41.4° N, 2.1° E, 125 m a.s.l.	UC	1077	0.22 ± 0.13	1.3 ± 0.3
Western Mediterranean Basin					
Avignon	43.9° N, 4.9° E, 32 m a.s.l.	U	1108	0.20 ± 0.13	1.4 ± 0.4
Toulon	43.1° N, 6.0° E, 50 m a.s.l.	UC	1146	0.20 ± 0.14	1.3 ± 0.5
Roma	41.8° N, 12.6° E, 130 m a.s.l.	U	949	0.24 ± 0.13	1.2 ± 0.4
Ispra	45.8° N, 8.6° E, 235 m a.s.l.	U	806	0.29 ± 0.23	1.4 ± 0.3
Lecce	40.3° N, 18.1° E, 30 m a.s.l.	UC	875	0.24 ± 0.14	1.2 ± 0.5
Blida	36.5° N, 2.9° E, 230 m a.s.l.	UC	1048	0.26 ± 0.17	0.9 ± 0.4
North-West Africa and Canary Islands					
Saada	31.6° N, 8.2° W, 420 m a.s.l.	D	1216	0.26 ± 0.17	0.7 ± 0.4
La Laguna	28.5° N, 16.3° E, 568 m a.s.l.	UC	837	0.17 ± 0.16	0.6 ± 0.3

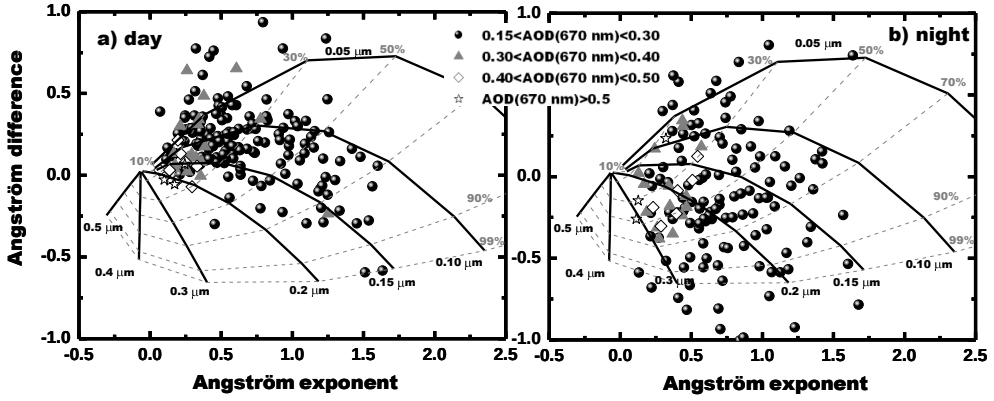

Fig. 4. (a) Angström exponent difference $\delta\alpha = \alpha$(440–670 nm) $-\alpha$(670–870 nm) as function of α(440–870 nm) at daytime and **(b)** Angström exponent difference $\delta\alpha = \alpha$(436–670 nm) $-\alpha$(670–880 nm) as function of α(436–880 nm) at nighttime. Both $\delta\alpha$ and the Angström exponents are the mean day or night values for the period 2007–2010. Different symbols indicate the ranges of aerosol optical depth at 670 nm used.

located in North Africa and is less affected by European air-masses. This station presents mean value of AOD(440 nm) of 0.26 ± 0.17 and mean value of α(440–870 nm) of 0.9 ± 0.4. These values are mainly explained by the large influence of Saharan air-masses and also by the increase of the anthropogenic activity in the Magreb countries (Rodríguez et al., 2011). The stations of Saada (in the North West of Africa) and La Laguna (Canary Islands) are quite affected by Saharan air-masses (e.g., Alastuey et al., 2005; Garcia et al., 2009), which explain their large values of AOD(440 nm) and low values of α(440–870 nm).

For the nighttime, to our knowledge currently there are no systematic measurements of AOD(λ) in the surrounding areas to our station and, thus, it is not possible to make any comparison. However, AOD(λ) and α mean values obtained in this work at nighttime are quite similar to those obtained during daytime (Table 1). But it is important to note that these findings are only relevant to sites with similar characteristics to that in the station of Granada.

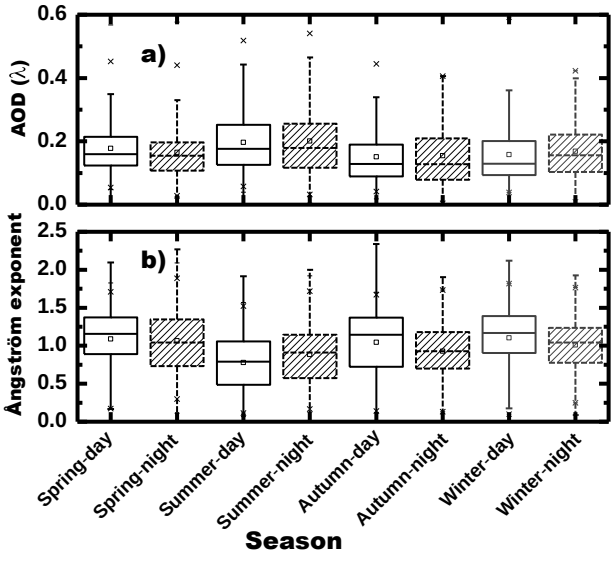

Fig. 5. Seasonal Box-Whisker diagrams of **(a)** AOD(440 nm) and AOD(436 nm) **(b)** α(440–870 nm) and α(436–880 nm) obtained at daytime and nighttime, respectively, during the period from 2007 to 2010 at the station of Granada. Dashed Box is for night-time data and empty Box is for day-time data. In these box diagrams the mean is represented by an open square. The line segment in the box is the median. The top limit represents the 75th percentile (P75) and the bottom limit the 25th percentile (P25). The box bars are related to the 1st (P1) and 99th (P99) percentiles, and the crosses represent the maximum and minimum values, respectively. The lines perpendicular to the box diagrams are 1.5 the interquartile range.

4.3 Seasonal evolution of aerosol optical properties

To analyse the seasonal variations of aerosol optical properties, the data are grouped in four seasons: winter (January, February and December of the previous year), spring (March, April and May), summer (June, July and August) and autumn (September, October and November). For the study period, Table 3 shows the seasonal mean values of AOD(440 nm) and α(440–870 nm) obtained at daytime, and AOD(436 nm) and α(436–880 nm) obtained nighttime.

Figure 5 shows the seasonal Box-Whisker diagrams of AOD(440 nm) and α(440–870 nm) obtained at daytime, and AOD(436 nm) and α(436–880 nm) obtained at nighttime during the study period. Figure 5a reveals an evident seasonal pattern in AOD(λ), characterised by large values in spring–summer and low values in autumn–winter. For α Fig. 5b also reveals a seasonal pattern characterised by low values in summer and in early-autumn and large values in winter and early spring, both at daytime and nighttime. Although there are no statistical differences between day and night seasonal patterns of AOD(λ) and α, according to the mean values of α (Table 3) this parameter shows slightly more remarkable pattern at daytime than at nighttime.

The seasonal patterns of AOD(λ) and α can be explained by several reasons. In late-spring, summer and early autumn, the higher frequency of Saharan dust intrusions in the study area and the low ventilation rates of air-masses in the Western-Mediterranean basin (e.g., Millan et al., 1997; Rodriguez et al., 2001; Lyamani et al., 2006a, b) can explain the large values of AOD(λ) and the relatively low values of α. Moreover, the intense atmospheric convective activity prevailing in this area in these months, together with the aridity of the soil during this particular period, provides a mineral dust (coarse particles) loading to the atmosphere from local soil. Another reason of these high AOD(λ) is the low rainfall rates, which are responsible of the aerosol load reduction. On the other hand, in late-autumn, winter and early-spring the aridity of the soil is quite reduced mainly by the rainfall and there are also less Saharan dust intrusions in the study area. In addition, the rain and clean Atlantic air-masses are more frequent in this period. All these reasons can explain the low values of AOD(λ) and large α values.

In the hot months the convective activity is more intense at daytime than at nighttime. As the convective activity ceases during the nighttime large particles can deposit, which can induce an increase in α (explaining their slightly larger values at nighttime). During the late-autumn and winter, local anthropogenic emissions are more relevant, which mainly supplies fine particles in the atmosphere. These emissions are more active during daytime, which can explain the larger values of α obtained during daytime compared to nighttime.

Figure 6 shows the frequency distributions of daytime and nighttime AOD(λ) and α for the different seasons. For AOD(440 nm) and AOD(436 nm) obtained at daytime and nighttime, respectively, all the distributions are unimodal with skewness at low AOD(λ) values. This skewness changes to slightly larger AOD(λ) values in summer. In all the seasons, the differences of the AOD(λ) modal values between daytime and nighttime are negligible. On the other hand, for α both at daytime and nighttime they present similar shape, and can be adjusted to a bimodal distribution. The first mode is $\sim$0.1–0.5 and can be associated with the presence of dust particles either from long range transport or local soil. Actually, this mode presents larger frequencies in summer when the influence of dust particles is more relevant. The second mode is observed at larger values of α ($\sim$1.1–1.4) and is associated with the presence of anthropogenic particles. Additionally, differences in the modal values of α can be observed between daytime and nighttime. But these differences are very low ($\sim$0.1) to obtain any conclusion about the changes in particle types between daytime and nighttime. Actually, only in autumn relevant differences are observed with the lack of the first mode at nighttime (corresponding to coarse particles), which can be associated with the presence of a strong Saharan dust outbreak on 6 September 2007 at daytime (Guerrero-Rascado et al., 2009). However, the study of $\delta\alpha$ can reveal further differences. In this sense, Fig. 7 and Fig. 8 show $\delta\alpha$ versus α at daytime and nighttime for summer

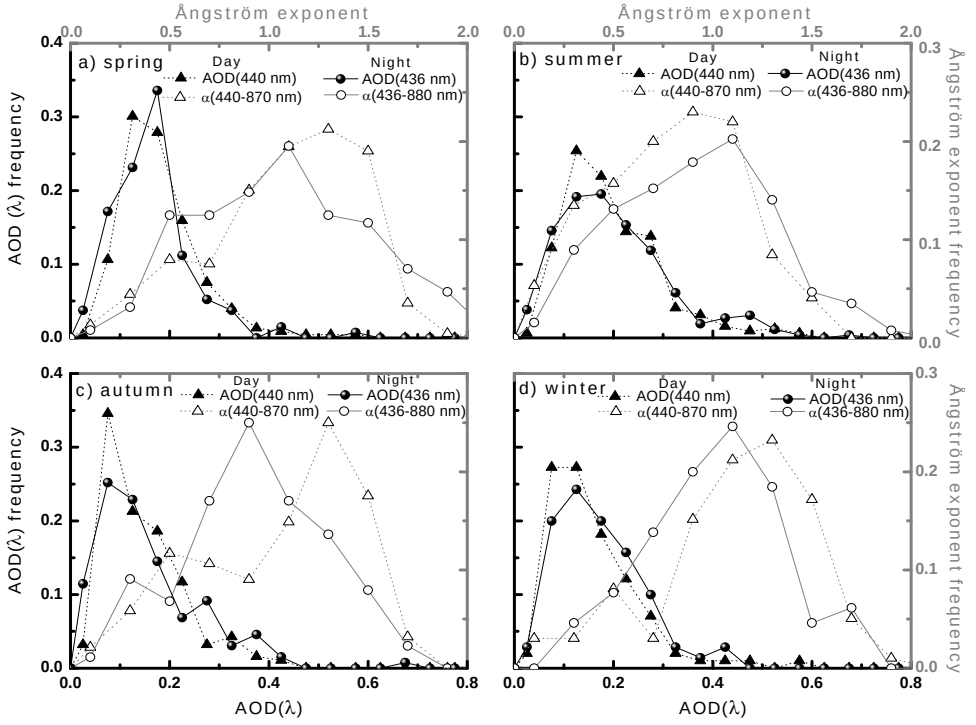

Fig. 6. Frequency histograms of AOD(440 nm) and α(440–870 nm) obtained at daytime and of AOD(436 nm) and α(436–880 nm) obtained at nighttime for: **(a)** spring **(b)** summer **(c)** autumn **(d)** winter.

Table 3. Seasonal mean values and standard deviations of AOD(λ) and Angström exponent α, obtained at daytime and nighttime at Granada.

		Mean values and standard deviations			
Parameter		Spring	Summer	Autumn	Winter
AOD(440 nm)	Day	0.18 ± 0.08	0.20 ± 0.10	0.15 ± 0.10	0.15 ± 0.10
AOD(436 nm)	Night	0.16 ± 0.08	0.20 ± 0.11	0.15 ± 0.11	0.17 ± 0.09
α(440–870 nm)	Day	1.1 ± 0.4	0.8 ± 0.4	1.0 ± 0.4	1.2 ± 0.4
α(436–880 nm)	Night	1.1 ± 0.4	0.9 ± 0.4	0.9 ± 0.4	1.0 ± 0.3

and winter season, respectively. We focus on these seasons to avoid the changeable synoptic and meteorological conditions in spring and autumn and, thus, study the differences in particle types between day and night for hot and cold months, respectively. Every point presented in the figures corresponds to a single measurement by the sun-photometer or 30 min average measurements by the star-photometer.

For the data plotted in Fig. 7, taking into account that only data with AOD(670 nm) > 0.15 are used, there are no important differences between daytime and nighttime AOD(λ). Actually, mean values of AOD(440 nm) at daytime are 0.34 ± 0.11, 0.33 ± 0.12, 0.30 ± 0.06, 0.32 ± 0.10 for the summers of 2007, 2008, 2009 and 2010, while during the nighttime mean AOD(436 nm) are 0.35 ± 0.11, 0.30 ± 0.09, 0.28 ± 0.07, 0.27 ± 0.09 for the summers of 2007, 2008, 2009 and 2010, respectively.

From Fig. 7 during the daytime, although there are differences among the different summers, two patterns of $\delta\alpha$ are clearly differentiated. The first one presents α(440–870 nm) < 0.5 and corresponds to $\eta < 30\,\%$, $r_f < 0.2\,\mu$m and $\delta\alpha > 0$. Backward-trajectories analysis and images of MODIS sensor on board of TERRA and AQUA satellites (http://modis.gsfc.nasa.gov) (graphs not shown) revealed that these data are mainly associated with Saharan dust intrusions. The work of Basart et al. (2009) showed that for sun-photometry measurements at the Sahara-Sahel deserts, mineral dust particles presented $\delta\alpha$ approximately between -0.5 and 0.1, $\alpha < 0.3$, $\eta < 40\,\%$ and $r_f \sim 0.3$. The differences between these values and those obtained in this study can be explained by the mixture of dust with local anthropogenic particles, and by the deposition of the larger particles during their transport to the study area. This pattern is more remarked

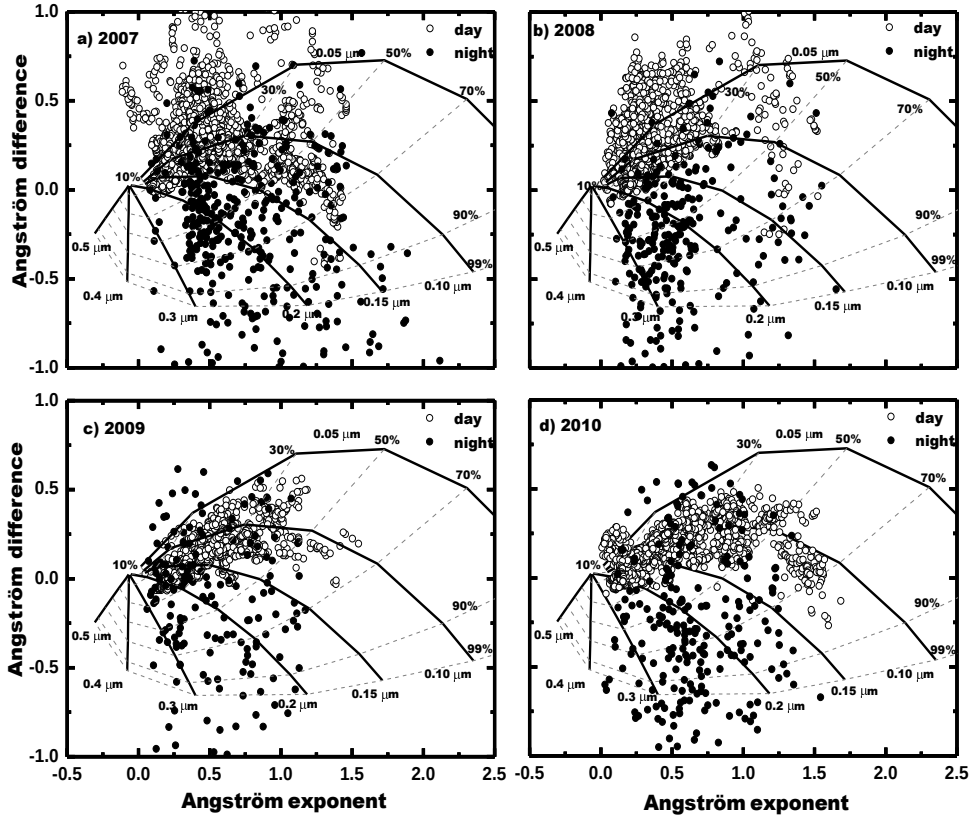

Fig. 7. Angström exponent difference $\delta\alpha = \alpha(440–670\,\text{nm}) - \alpha(670–870\,\text{nm})$ as function of $\alpha(440–870\,\text{nm})$ at daytime and $\delta\alpha = \alpha(436–670\,\text{nm}) - \alpha(670–880\,\text{nm})$ as function of $\alpha(436–880\,\text{nm})$ at nighttime, for summer season. **(a)** For year 2007. **(b)** For year 2008. **(c)** For year 2009. **(d)** For year 2010. Each point presented in that figure corresponds to a single measurement with sun-photometry or 30 min average measurements with star-photometry.

during the years 2007 and 2008 which was affected by more intense and frequent Saharan dust outbreaks.

The second pattern is characterised by $\alpha(440–870\,\text{nm}) > 0.75$, and most of the data present $\delta\alpha > 0$ and η of $\sim$30–70 %, and r_f of $\sim$0.10–0.15 µm. These data are usually associated with predominance of fine particles (e.g., Basart et al., 2009). Particularly, the influence of sporadic biomass-burning events in this season and anthropogenic particles transported from polluted Mediterranean and European areas can explain these values of $\delta\alpha$, $\alpha(440–870\,\text{nm})$ and η (e.g., Lyamani et al., 2006a, b; Alados-Arboledas et al., 2011). In fact, in summers 2009 and 2010 the larger influence of continental and Mediterranean air-masses explains the larger presence of this pattern. The clustering is toward a r_f line and the extension to higher AOD happens perpendicular the r_f line, into larger fine mode fraction. This indicates growth of the fine mode by aging processes (Gobbi et al., 2007). The study of Gobbi et al. (2007) also showed patterns like that one for highly polluted places like Beijing (China), Kanpur (India), Ispra (Italy), Mexico DC (Mexico) or Goddard Space Flight Centre (USA).

During nighttime, the two patterns of daytime data in Fig. 7 are not observed, being found a clockwise rotation of the data (η ranging from 30 to 99 %, r_f ranging from 0.1 to 0.3 µm and $\delta\alpha < 0$). This implies changes in the fine mode particle characteristics between daytime and nighttime. Although quick changes of the synoptic conditions between day and night can be found, no systematic differences of day-to-night air-masses affecting the study area are expected and, thus, differences of air-masses can not explain these day-to-night changes. The supply of local mineral particle from the ground during daytime by the strong convective activity can explain the lower values of η. The increase of r_f at nighttime can be explained by aerosol aging processes such as coagulation and condensation (Seinfeld and Pandis, 1998). The combined increase in η and r_f can be associated with hygroscopic growth (Gobbi et al., 2007). Although the relative humidity at the surface is low ($\sim$ 50 %), larger values can be obtained at higher altitudes and favour hygroscopic growth processes. However, we must be careful about this statement because of the absence of relative humidity vertical profiles, information about mixing conditions and aerosol

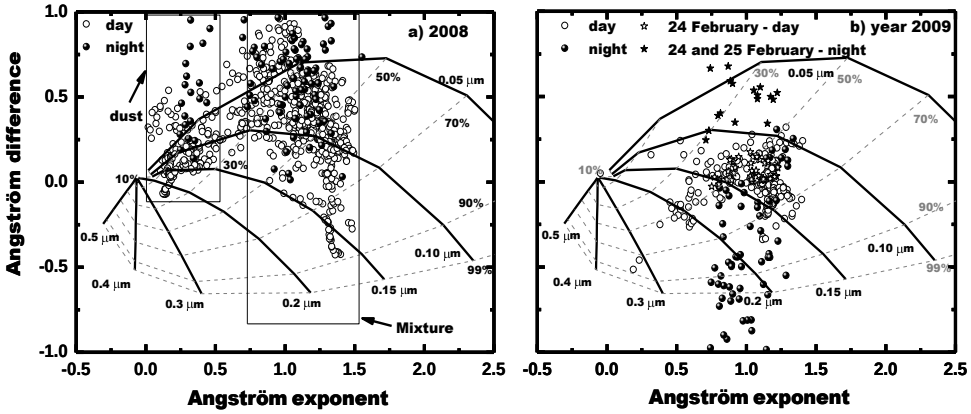

Fig. 8. Angström exponent difference $\delta\alpha = \alpha(440–670\,\text{nm}) - \alpha(670–870\,\text{nm})$ as function of $\alpha(440–870\,\text{nm})$ at daytime and $\delta\alpha = \alpha(436–670\,\text{nm}) - \alpha(670–880\,\text{nm})$ as function of $\alpha(436–880\,\text{nm})$ at nighttime, for the winter season. **(a)** For year 2008. **(b)** For year 2009. Each point presented in that figure corresponds to a single measurement with sun-photometry or 30 min average measurements with star-photometry.

vertical distribution. Many processes compete, and the use of the Gobbi diagrams does not allow their separation.

For the winter season, Fig.8 shows the results in 2008 and 2009 (in winter 2007 the star photometer was not available, while bad meteorological conditions during winter 2010 explain the lack of data). There are no very large differences of AOD(λ) between both years. For the data plotted in Fig. 8a mean value of AOD(440 nm) is 0.22 ± 0.09 at daytime, while during nighttime mean value of AOD(436 nm) is 0.21 ± 0.06. On the other hand, for the data presented in Fig. 8b, mean AOD(440 nm) is 0.26 ± 0.14 at daytime and mean AOD(436 nm) is 0.28 ± 0.10 at nighttime. However, the patterns of $\delta\alpha$ versus α between both years are very different.

The inter-annual variation of the air-masses affecting the study area explains the differences of the aerosol particles between 2008 and 2009. According to the five-day backward-trajectories analysis and MODIS satellite images, during the late winter of 2008 some Saharan dust intrusions affected the study area (approximately 35 % of the days and nights used in Fig. 8a). From Fig. 8a, at daytime two patterns can be observed. The first one presents $\delta\alpha > 0$, $\alpha < 0.5$, $\eta < 30\,\%$ and $r_\text{f} < 0.2\,\mu\text{m}$, and is mainly associated with dust particles transported from North Africa. The second one is characterised by $\delta\alpha > -0.5$, $\alpha > 0.75$, η up to 90 % and most data with r_f below 0.15 µm. This last pattern is associated with a mixture of different aerosol types, both mineral dust and anthropogenic particles. For nighttime, the two patterns previously mentioned are also observed and in both cases η values are lower than those observed at daytime. As commented before, anthropogenic emissions are more active during the daytime than during the nighttime, and can explain the predominance of the fine mode particles at daytime. This result is in good agreement with the comment before about the slightly larger values of α observed during daytime in winter (Fig. 5b).

In winter 2009 (Fig. 8b) the synoptic conditions were different to those in 2008, with a lot of rain periods. The AOD(670 nm) > 0.15 were obtained only during the period from 18 to 26 February. For this short period, the air-masses affecting the study area were mainly of continental origin. Particularly, larger values of η and r_f are obtained at nighttime. During the daytime, η ranges between 30 % and 70 %, r_f between 0.1 µm and 0.2 µm, and $\delta\alpha$ between -0.25 and 0.25, while at nighttime η ranges between 50 % and 99 %, r_f between 0.15 µm and 0.25 µm, and $\delta\alpha$ between -0.75 and 0.1. Aging processes can again explain this increase of the fine mode radius. Particularly the hygroscopic growth is an important factor at high relative humidity for anthropogenic particles (e.g., Kotchenruther et al., 1999; Raut and Chazette, 2007; Randriamiarisoa et al., 2006; Veselovskii et al., 2009). But again we have to insist on the limitations of the methodology proposed that does not allow the separation between any processes. On the other hand, from 24 to 25 February (stars symbol in Fig. 8b) there were quick and intense pollution plumes associated with air-masses originated in the European continent and in the Mediterranean Sea, which can explain the differences of r_f and η to those observed for the other days and nights during this winter.

The differences in the results between years 2008 and 2009 do not allow for the obtaining of any conclusion about the day-to-night aerosol types in winter. It is associated with the complexity of the atmosphere during this season at the study area, which includes changes in the synoptic conditions, in the planetary boundary layer and in aerosol emission sources.

4.4 Columnar aerosol properties dynamic: study cases

The comment above showed the similarity in AOD(λ) and α between daytime and nighttime for aerosol climatology. In spite of the continuity in the mean values, shorter time scales are needed to study "day-to-night" aerosol dynamic

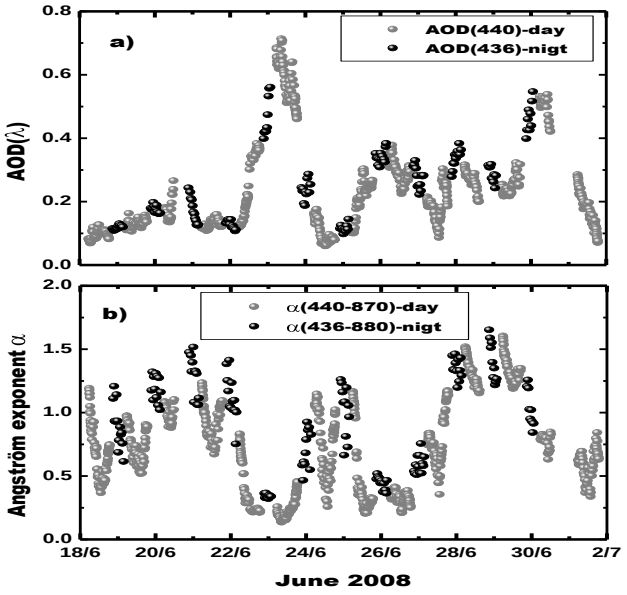

Fig. 9. Daytime and nighttime evolutions of columnar aerosol properties for the period from 18 June to 2 July 2008. **(a)** Aerosol optical depth (AOD). **(b)** Angström exponent α.

and also to know the effects of the changes of the air-masses. Two studies are presented focussing on summer and winter seasons with very different atmosphere characteristics.

4.4.1 (a) Summer season: 18 June–2 July 2008

Figure 9 shows, for the period between 18 June and 2 July 2008, the time evolutions of AOD(440 nm) at daytime and AOD(436 nm) at nighttime (Fig. 9a), and also time evolutions of α(436–880 nm) at daytime and α(436–880 nm) at nighttime (Fig. 9b).

From Fig. 9 can be observed a good continuity in day-to-night AOD(λ) values. Similar continuity is also observed in α (Fig. 9b). Mean values of AOD(λ) and α and the origin of the air-masses for the days and nights of Fig. 9 are showed in Table 4. As can be observed mean values of AOD(440 nm) and α(440–870 nm) at daytime are similar to those obtained at nighttime, with smooth variations in day-to-night evolutions. Day-to-night differences between mean values are remarkable only when there are changes in the origins of the air-masses between day and night, although these variations of AOD(λ) and α are coherent with the smooth time evolutions showed in Fig. 9. However, the variability in the air-mass affecting the study area induces important differences in the day-to-day and night-to-night evolutions of AOD(λ) and α. Atlantic air-masses present low AOD(λ) while those from Sahara desert present large AOD(λ) and low values of α. Continental and Mediterranean air-masses are usually responsible of large values of AOD(λ) and α.

On 18 June the study area was affected by Atlantic air-masses while on the following days and nights, the air-masses came from the North of Morocco and later from the South of the Iberian Peninsula with implies changes in the time-evolutions (Fig. 9), increasing AOD(λ) (maximum values up to 0.25 on 20 June) and α (maximum values up to 1.5 on 20 June). On 22 and 23 June the air-masses affecting the area were originated in the Sahara desert transporting mineral dust particles and inducing a sharp increase of AOD(436 nm) on 22–23 June night (maximum values up to 0.7), while the posterior changes to Atlantic air-masses cleaned the atmosphere explaining the sharp decrease of AOD(λ) (minimum values down to 0.14). From 25 June afternoon the air-masses over the study area changed to those with origin in the Iberian Peninsula increasing the aerosol load. However, α reaches very low values ($\sim$ 0.45) that in the study area are usually associated with long-range transport of Saharan dust particles (Lyamani et al., 2005, 2006; Valenzuela et al., 2012a, b). The more in depth analysis of backward-trajectories for this night revealed that the air-masses reaching the study area at 4000 m a.s.l. on 25, 26 and 27 June came from the Sahara desert. In this sense, the work of Guerrero-Rascado et al. (2009) showed that long-range transport of mineral Saharan dust particles can reach altitudes above 3000 m a.s.l. in the study area. For this particular case, range corrected signals of correlative lidar measurements during these days and nights showed strong backscattered signal at these high altitudes (graphs not shown, but can be consulted at http://atmosferera.ugr.es). Therefore, presence of Saharan dust particles at these altitudes can explain the low values of α for these days and nights.

On 27–28 June night, the air-mass precedence moves to the East, with origin between the South of the Iberian Peninsula and the North African countries. No transport of Saharan dust particles is observed (again by checking correlative lidar measurements), and α(436–880 nm) increases ($\sim$ 1.2–1.5). These values of α can be explained by the increase in the anthropogenic emissions in the North Africa countries (Rodríguez et al., 2011). From 28 June to 1 July the study area was affected by Mediterranean air-masses which are associated with very variable aerosol loads and types (Pandolfi et al., 2011) because this sea can be a reservoir of pollutants from the surrounding countries (Lyamani et al., 2006; Rodríguez et al., 2011) and also of dust particles transported from the Sahara desert (Meloni et al., 2007; Rodríguez et al., 2011). During this short period, large AOD(λ) remain. However, there is variability of α. Until 29 June large values of α (values up to 1.6) suggest predominance of fine particles associated with anthropogenic particles, while the decrease of α from late 29 to early 30 June (values $\sim$ 0.75) suggest some influence of Saharan dust particles over the Mediterranean. This last has been checked by MODIS images and also explains the sharp increase of AOD(λ) (maximum values up to 0.55 on 30 June). Finally, the decrease of AOD(λ)

Table 4. Mean values of day- and night-time aerosol optical depth (AOD) and Angström exponent as well as the associated air-mass types that affected the study area for every day and night between 18 June and 1 July 2008. Air-masses backward-trajectories were computed by HYSPLIT model at 1500 m a.g.l.

Day-time				Night-time			
Date (2008)	AOD(440 nm)	α(440–870 nm)	Air-mass origin	Date (2008)	AOD(440 nm)	α(440–870 nm)	Air-mass origin
18 June	0.09 ± 0.01	0.69 ± 0.22	North Atlantic	18–19 June	0.12 ± 0.01	0.88 ± 0.18	South Atlantic
19 June	0.15 ± 0.01	0.79 ± 0.13	North Africa	19–20 June	0.18 ± 0.01	1.19 ± 0.10	North Africa
20 June	0.17 ± 0.01	1.00 ± 0.07	Iberian Peninsula	20–21 June	0.17 ± 0.04	1.13 ± 0.06	North Africa
21 June	0.13 ± 0.01	1.01 ± 0.07	Iberian Peninsula	21–22 June	0.13 ± 0.01	1.09 ± 0.07	Iberian Peninsula
22 June	0.24 ± 0.11	0.40 ± 0.21	Sahara Desert	22–23 June	0.34 ± 0.02	0.47 ± 0.06	Sahara Desert
23 June	0.58 ± 0.07	0.24 ± 0.09	Sahara Desert	23–24 June	0.24 ± 0.03	0.71 ± 0.16	South Atlantic
24 June	0.15 ± 0.02	1.04 ± 0.07	South Atlantic	24–25 June	0.13 ± 0.02	1.06 ± 0.18	South Atlantic
25 June	0.21 ± 0.06	0.5 ± 0.3	South Atlantic	25–26 June	0.34 ± 0.02	0.44 ± 0.05	Iberian Peninsula
26 June	0.30 ± 0.04	0.33 ± 0.04	Iberian Peninsula	26–27 June	0.28 ± 0.03	0.59 ± 0.07	Iberian Peninsula
27 June	0.22 ± 0.18	0.89 ± 0.18	Iberian Peninsula	27–28 June	0.33 ± 0.04	1.35 ± 0.08	North Africa
28 June	0.28 ± 0.02	1.36 ± 0.09	Iberian Peninsula	28–29 June	0.29 ± 0.03	1.40 ± 0.14	Mediterranean Sea
29 June	0.25 ± 0.03	1.35 ± 0.11	Mediterranean Sea	29–30 June	0.46 ± 0.05	1.03 ± 0.09	Mediterranean Sea
30 June	0.50 ± 0.03	0.78 ± 0.05	Mediterranean Sea	30 June–1 July	–	–	Mediterranean Sea
1 July	0.22 ± 0.03	0.56 ± 0.11	Atlantic	1–2 July	–	–	Atlantic

Table 5. Mean values of day- and night-time aerosol optical depth (AOD) and Angström exponent as well as the associated air-mass types that affected the study area for every day and night between 21 January and 1 February 2008. Air-masses backward-trajectories were computed by HYSPLIT model at 1500 m a.g.l.

Day-time				Night-time			
Date (2008)	AOD(440 nm)	α(440–870 nm)	Air mass origin	Date (2008)	AOD(440 nm)	α(440–870 nm)	Air mass origin
21 January	0.08 ± 0.02	1.05 ± 0.18	European Continent	21–22 January	0.11 ± 0.02	1.14 ± 0.20	Iberian Peninsula
22 January	0.12 ± 0.02	1.21 ± 0.05	North Atlantic	22–23 January	0.16 ± 0.05	0.70 ± 0.14	North Atlantic
23 January	0.09 ± 0.02	0.95 ± 0.11	North Atlantic	23–24 January	0.17 ± 0.02	0.66 ± 0.14	North Atlantic
24 January	0.21 ± 0.02	0.82 ± 0.24	North Atlantic	24–25 January	0.19 ± 0.03	0.92 ± 0.18	North Atlantic
25 January	0.27 ± 0.03	0.82 ± 0.17	Atlantic – Iberian Peninsula	25–26 January	–	–	European Continent
26 January	0.20 ± 0.03	1.20 ± 0.14	European Continent	26–27 January	0.23 ± 0.05	1.06 ± 0.08	European Continent
27 January	0.19 ± 0.03	1.28 ± 0.10	European Continent	27–28 January	0.24 ± 0.06	1.28 ± 0.15	European Continent
28 January	0.21 ± 0.02	1.36 ± 0.08	Mediterranean Sea	28–29 January	0.21 ± 0.02	1.08 ± 0.13	Mediterranean Sea – North Africa
29 January	0.20 ± 0.03	1.26 ± 0.10	Mediterranean Sea	29–30 January	0.21 ± 0.05	1.11 ± 0.17	Local
30 January	0.12 ± 0.03	1.02 ± 0.17	Iberian Peninsula	30–31 January	0.15 ± 0.02	0.97 ± 0.08	Atlantic – Iberian Peninsula
31 January	0.15 ± 0.03	1.05 ± 0.13	Iberian Peninsula	31 January–1 February	0.19 ± 0.02	1.09 ± 0.13	Iberian Peninsula
1 February	0.16 ± 0.03	1.11 ± 0.18	North Atlantic	1–2 February	–	–	North Atlantic

(values down to 0.1) during the following days and nights is explained by the changes towards North Atlantic air-masses.

In spite of the continuity of α between daytime and nighttime, the changes in the day-to-night evolutions make us study the behaviour of α in detail. In this sense, Fig. 10 shows $\delta\alpha$ versus α for the data showed in Fig. 9, both at daytime and nighttime.

From 19 to 20 June (Fig. 10a, b, c) with relatively low aerosol load, α is larger than 1 both at daytime and nighttime, but there are remarkable differences in $\delta\alpha$. Daytime values present $r_f < 0.1$ µm and $\eta < 50$ %, being around one half of the data with $\eta < 30$ %. However, during nighttime the pattern is very different, presenting all the data $r_f > 0.1$ µm and $\eta > 50$ %, and around one half of data with $r_f > 0.15$ µm and $\eta > 75$ %. On 22 and 23 June (Fig. 10d, e), with presence of Saharan dust particles, at daytime r_f is lower than 0.15 µm and η lower than 30 %, while at nighttime the opposite occurs ($r_f > 0.15$ µm and $\eta > 30$ %). On 24 June (Fig. 10f) the Atlantic air-masses affecting the study area induced lower aerosol load and larger α values, being the values of r_f and η similar to those just discussed for Fig. 10a, b, c.

From 25 afternoon to 27 morning, (with dust particles above 3000 m a.s.l.) Fig. 10g, h shows that at daytime r_f is lower than 0.15 µm, and η is below than 30 % on 25 and 26 June (except some data at the beginning of 25 June associated with the changes in the air-masses), and below 50 % on 27 June. During nighttimes there are again differences with larger values of r_f (values up to 0.3 µm) and η (up to 90 %). On the night of 27–28, there were changes of the air-masses that induces larger values of r_f and η as well. For the following period from 28 to 29 June affected by transport of fine particles from the Mediterranean sea, Fig. 10j, k show

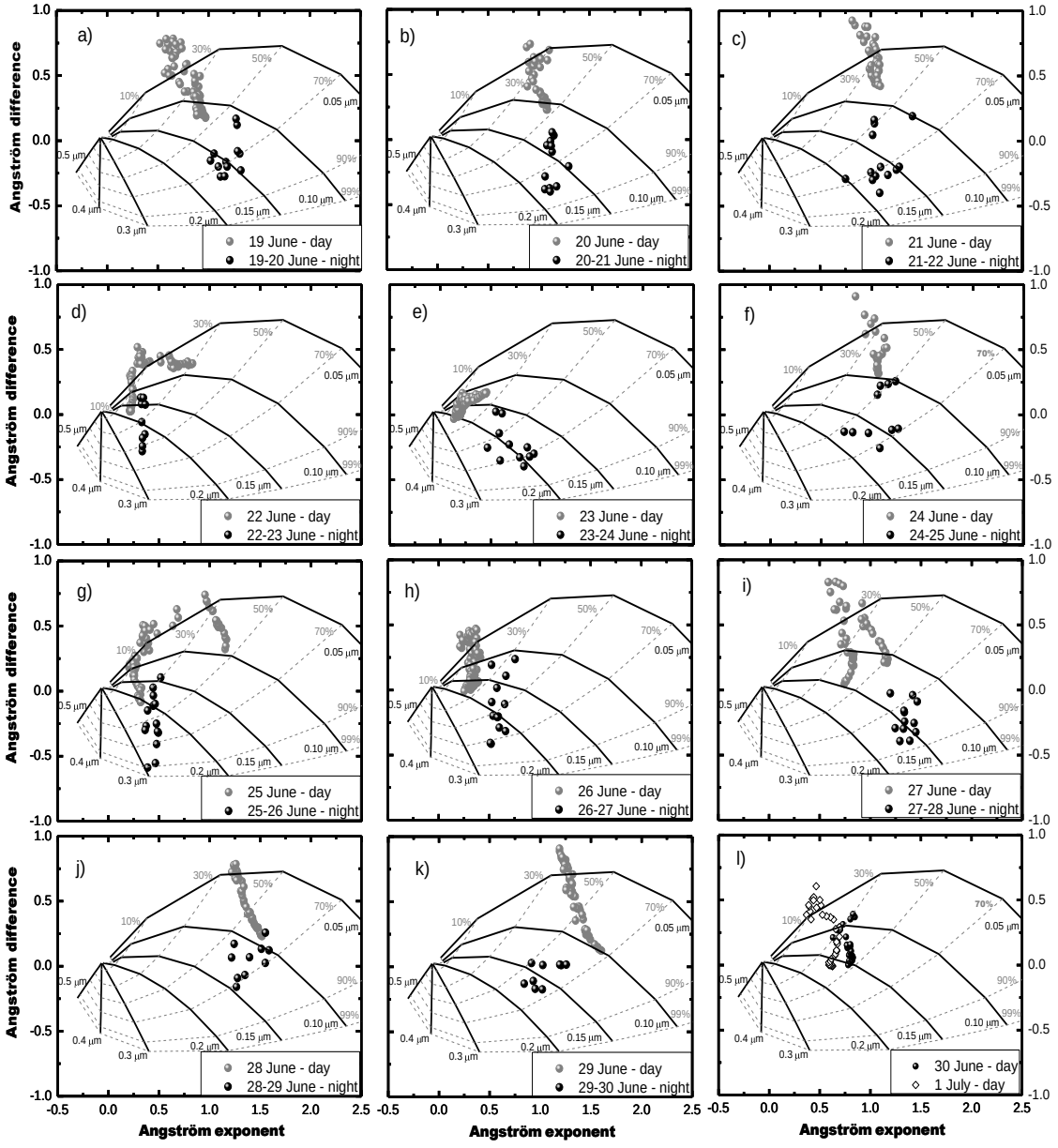

Fig. 10. Angström exponent difference $\delta\alpha = \alpha(440\text{–}670\,\text{nm}) - \alpha(670\text{–}870\,\text{nm})$ as function of $\alpha(440\text{–}870\,\text{nm})$ at daytime and $\delta\alpha = \alpha(436\text{–}670\,\text{nm}) - \alpha(670\text{–}880\,\text{nm})$ as function of $\alpha(436\text{–}880\,\text{nm})$ at nighttime, for summer case study. The data corresponds to the period from 18 June to 1 July 2008.

at daytime $r_f < 0.1\,\mu\text{m}$ and $\eta < 70\,\%$. The more variability of η on these days might be associated with the contribution of coarse particles from the ground as the convective activity increase. On the night of 28–29, η does not change significantly, but r_f present important changes toward larger values (between 0.15 and 0.20 µm). Finally, on the night of 29–30 June and on 30 June (daytime) the Mediterranean air-masses transported Saharan dust particles. In this case, the pattern observed is again of larger values of r_f and η during the nighttime.

The findings of Fig. 10 reveal increases of r_f and of η during nighttime for the different aerosol loads and types. This has been found for different types of air-masses, and also when there are changes in the air-masses between day and night. These results also agree with the general results obtained in Fig. 7 for the summer season, and can be explained by the same reasons. Again, with the methodology used here we can not differentiate between the different processes that induce changes in particle types between day and night.

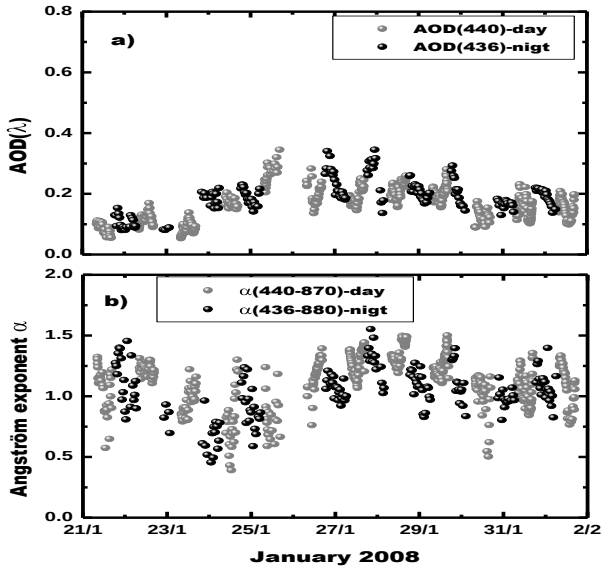

Fig. 11. Daytime and nighttime evolutions of columnar aerosol properties for the period from 21 January to 2 February 2008. **(a)** Aerosol optical depth (AOD). **(b)** Angström exponent α.

4.4.2 (b) Winter season: 21 January–1 February 2008

Figure 11 shows for the period between 21 January and 1 February 2008 the temporal evolutions of AOD(440 nm) at daytime and AOD(436 nm) at nighttime (Fig. 11a), and also temporal evolutions of α(436–880 nm) at daytime and α(436–880 nm) at nighttime (Fig. 11b). Table 5 shows mean values of AOD(λ) and α, and also the origin of the air-masses for these days and nights.

Again, from Fig. 11, we can observe a good continuity in day-to-night evolutions of AOD(λ) and α. Particularly, α is usually slightly lower at nighttime and agrees with the comment in Fig. 5 for the winter season. The larger errors in AOD(λ) at nighttime can explain the fluctuations of α in the nights with low aerosol load (error in α are larger for low AOD(λ)).

As for the previous study case during the summer, mean values of AOD and α at daytime are similar to those obtained at nighttime and only the differences are notable when changes in the air-masses origin are presented (although the differences are smoothed as shown in Fig. 11). However, there are again large day-to-day and night-to-night variations associated with the changes of the air-masses that reach the study area. On 21 January the air-masses that affected the study area were from European origin. On 22–25 January the study area was under the influence of clean Atlantic air-masses, which explain the low aerosol loads (AOD(λ) < 0.2 for these days and nights) with large variability of α.

From 26 to 29 January the situation changed and the air-masses came from the European and Mediterranean sectors which transported anthropogenic particles to the study area. These air-masses produced an increase of AOD(λ) and α (Table 5). The larger aerosol loads during these days and nights allow the study of $\delta\alpha$ versus α (Fig. 12). On 26 January, at day time, it is observed that $\delta\alpha > 0$, $r_f < 0.1$ µm and η between 30 % and 50 % (Fig. 12a). However, at nighttime we observe $\delta\alpha > 0$ and most data present $r_f < 0.1$ µm and $\eta < 30$ %. On 27 January very similar results to those obtained in the previous day and night are observed (Fig. 12b). The larger contribution of fine mode particles at daytime can be explained by the larger anthropogenic emissions during daytime. It is worth noting that although r_f is very small (< 0.1 µm) both at daytime and nighttime (Fig. 12), daytime values are generally larger than nighttime ones, which can be explained by the contribution of larger particles by road traffic or by secondary aerosol originated from primary anthropogenic emissions (Lyamani et al., 2010).

On 28 and 29 January the study area was under the influence of Mediterranean air-masses influence, with large values of α (between 1.2 and 1.5 at daytime and from 0.8 to 1.35 at night-time) indicating the predominance of fine particles. Furthermore, on 28–29 January r_f and η patterns are similar to those obtained on 26 and 27 January (Fig. 12c). Finally, from 30 January to 1 February the air-masses precedence changed to Atlantic which made AOD(λ) and α decrease.

This study case remarked the continuity of day-to-night columnar aerosol properties in winter, but do not allow conclusions about the $\delta\alpha$. Indeed, together with Fig. 8, remarked the complexity of any general conclusion for winter due to the presence of different aerosol types, different intensity of aerosol aerosol sources (natural and anthropogenic) and differences in the atmosphere's temperature in planetary boundary layer and the changeable synoptic conditions in terms of rain and wind velocity. Thus, more efforts are needed using high technology instrumentations to characterise vertical atmosphere thermodynamics and vertical aerosol properties.

5 Conclusions

An analysis of correlative day-to-night columnar aerosol properties at Granada (South-East of Spain) has been presented. This study was possible thanks to the recent developments in star photometry combined with the well-known sun photometry technique (particularly using the CIMEL instrument). The combination of correlative measurements with both techniques has allowed the study of day-to-night aerosol optical depth (AOD), Angström exponent α, and spectral dependence of the Angström exponent ($\delta\alpha$).

Time evolutions of AOD and α have revealed good continuity and coherence between daytime and nighttime values, both for the whole database and for special study cases. Moreover, the statistical analyses have shown no significant differences between daytime and nighttime for both parameters. For daytime values, the comparison carried out with other AERONET surrounded stations has revealed that the

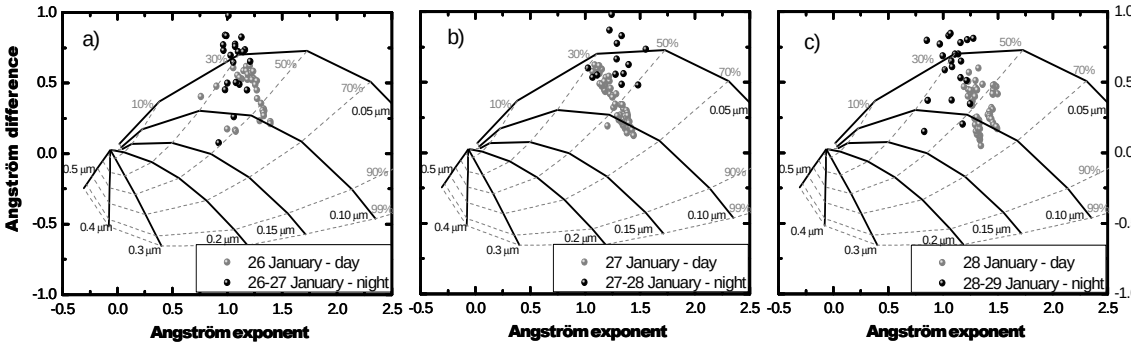

Fig. 12. Angström exponent difference $\delta\alpha = \alpha(440–670\,\text{nm}) - \alpha(670–870\,\text{nm})$ as function of $\alpha(440–870\,\text{nm})$ at daytime and $\delta\alpha = \alpha(436–670\,\text{nm}) - \alpha(670–880\,\text{nm})$ as function of $\alpha(436–880\,\text{nm})$ at nighttime, for a winter case study. The data corresponds to the period from 26 to 29 January 2008.

values obtained at Granada do not by differentiate remarkably with those obtained in the surrounded areas, in spite of the differences in synoptic conditions and aerosol sources. However, at nighttime no comparisons have been possible due to the lack of continuous measurements and, thus, the continuity observed in the long-term columnar aerosol properties at Granada cannot be extrapolated to other aerosol sites because of differences in meteorological conditions and aerosol sources. In this sense, the development of continuous nighttime measurements worldwide is needed to better understand aerosol dynamics globally.

A seasonal pattern for AOD has been obtained, both at daytime and nighttime, characterised by lower values in winter and larger values in summer. The Angström exponent has also presented a seasonal pattern but with lower values in summer and larger values in winter. No statistical differences in AOD and α seasonal pattern between day and night have been found out. These patterns have been associated with the different soil conditions at each season, with changes in the synoptic conditions and rainfall, and with the intensity of the local aerosol sources.

The spectral difference of the Angström exponent ($\delta\alpha$) as function of α has been studied, both at daytime and nighttime. Particular studies cases have showed the evolution of $\delta\alpha$ detailed. In summer, an increase of the fine mode radius (r_f) and of the fine mode contribution to AOD (η) has been observed at nighttime. This has been obtained for many different air-masses and aerosol loads and types, and has been explained by the changes of the local aerosol source emissions and meteorological conditions between daytime and nighttime. Moreover, the increase of r_f during nighttime has been also associated with aerosol aging processes. In the winter season, for $\delta\alpha$ the situation is more complex due to the more variability of the synoptic conditions and aerosol sources. For low-polluted aerosol load, the special cases analysed have shown larger r_f and η during daytime. It has been associated with the more intensive local anthropogenic sources, aerosol secondary aerosol formation and ground-based particles supplies by traffic. However, for highly polluted air-masses it is observed just the opposite, with an increase of r_f and η at nighttime. This has been explained by aging processes or deposition of coarse particles during air-mass transport. However, the reduced data points obtained under these conditions make us be careful. We would like to remark that the study of spectral variation of α alone does not allow distinguishing between different aerosol aging processes. Many of such processes compete, including changes in the aerosol load due to meteorological conditions, dry/wet deposition, coagulation/condensation processes, hygroscopic growth or the supply of particles from the ground or from anthropogenic activities.

The results presented allow the scientific community to advance in the knowledge of day-to-night columnar aerosol dynamics, both for large database and shorter temporal scales. However, we would like to point out that the differences between daytime and nighttime aerosol particles are only referred to a particular site with particular conditions, and these results cannot be extrapolated to any other place. In this sense, more efforts of the scientific community should be done to improve the knowledge of columnar aerosol properties at nighttime.

Acknowledgements. This work was supported by the Spanish Ministry of Science and Technology through projects CGL2008-01330-E/CLI (Spanish Lidar Network), CGL2010-18782, CSD2007-00067 and CGL2011-13580-E/CLI; by the Andalusian Regional Government through projects P10-RNM-6299 and P08-RNM-3568; by the EU ACTRIS project (EU INFRA-2010-1.1.16-262254), and by the Postdoctoral Programme of the University of Granada. The authors would like to express their gratitude to the NASA Goddard Space Flight Center, NOAA Air Resources Laboratory and Naval Research Laboratory for the HYSPLIT model. We also thank AERONET network and especially the principal investigators of the stations used for their efforts in establishing and maintaining the AERONET sites. We also express our gratitude to the anonymous referees and to the editor for their suggestions to improve this work.

Edited by: E. Gerasopoulos

References

Alados-Arboledas, L., Lyamani, H., and Olmo, F. J.: Aerosol size properties at Armilla, Granada (Spain), Q. J. Roy. Meteorol. Soc., 129, 1395–1413, doi:10.1256/qj.01.207, 2003.

Alados-Arboledas, L., Alcántara, A., Olmo, F. J., Martínez-Lozano, J. A., Estellés, V., Cachorro, V., Silva, A. M., Horvath, H., Gangl, M., Díaz, A., Pujadas, M., Lorente, J., Labajo, A., Sorribas, M., and Pavese, G.: Aerosol columnar properties retrieved from CIMEL radiometers during VELETA 2002, Atmos. Environ., 42, 2654–2667, 2008.

Alados-Arboledas, L., Muller, D., Guerrero-Rascado, J. L., Navas-Guzman, F., Perez-Ramirez, D., and Olmo, F. J.: Optical and microphysical properties of fresh biomass burning aerosol retrieved by Raman lidar, and star-and sun-photometry, Geophys. Res. Lett., 38, L01807, doi:10.1029/2010gl045999, 2011.

Alastuey, A., Querol, X., Castillo, S., Escudero, M., Avila, A., Cuevas, E., Torres, C., Romero, P. M., Exposito, F., García, O., Díaz, J. P., van Dingenen, R., and Putaud, J.: Characterisation of TSP and PM2.5 at Izaña and Sta. Cruz de Tenerife (Canary Islands, Spain) during a Saharan Dust Episode (July 2002), Atmos. Environ., 39, 4715–4728, 2005.

Baibakov, K., O'Neill, N. T., Firanski, B., and Strawbridge, K.: Preliminary Analysis of Night-time Aerosol Optical Depth Retrievals at a Rural, Near-urban Site in Southern Canada, in: Current Problems in Atmospheric Radiation, edited by: Nakajima, T. and Yamasoe, M. A., AIP Conference Proceedings, 443–446, 2009.

Basart, S., Pérez, C., Cuevas, E., Baldasano, J. M., and Gobbi, G. P.: Aerosol characterization in Northern Africa, Northeastern Atlantic, Mediterranean Basin and Middle East from direct-sun AERONET observations, Atmos. Chem. Phys., 9, 8265–8282, doi:10.5194/acp-9-8265-2009, 2009.

Bennouna, Y. S., Cachorro, V. E., Toledano, C., Berjon, A., Prats, N., Fuertes, D., Gonzalez, R., Rodrigo, R., Torres, B., and de Frutos, A. M.: Comparison of atmospheric aerosol climatologies over southwestern Spain derived from AERONET and MODIS, Remote Sens. Environ., 115, 1272–1284, doi:10.1016/j.rse.2011.01.011, 2011.

Berkoff, T. A., Sorokin, M., Stone, T., Eck, T. F., Hoff, R., Welton, E., and Holben, B.: Nocturnal aerosol optical depth measurements with a small-aperture automated photometer using the moon as a light source, J. Atmos. Oceanic Technol., 28, 1297–1306, doi:10.1175/JTECH-D-10-05036.1, 2011.

Bösenberg, J., Ansmann, A., Baldasano, J. M., Balis, D., Böckmann, C., Calpini, B., Chaikovsky, A., Flamant, P., Hagard, A., Mitev, A., Papayannis, A., Pelon, J., Resendes, D., Schneider, J., Spinelli, N., Trickl, T., Vaughan, G., Visconti, G., and Wiegner, M.: EARLINET: a European aerosol research lidar network, laser remote sensing of the atmosphere", in: Selected Papers of the 20th International Laser Radar Conference, Edition Ecole Polytechnique, Palaiseau, France, 155–158, 2001.

Brunekreef, B. and Forsberg, B.: Epidemiological evidence of effects of coarse airborne particles on health, European Respiratory Journal, 26, 309–318, doi:10.1183/09031936.05.00001805, 2005.

Cachorro, V., Toledano, C., Prats, N., Sorribas, M., Mogo, S., Berjón, A., Torres, B., Rodrigo, R., de la Rosa, J., and De Frutos, A. M.: The strongest desert dust intrusion mixed with smoke over the Iberian Peninsula registered with Sun photometry, J. Geophys. Res.-Atmos., 113, D14S04, doi:10.1029/2007JD009582, 2008.

Córdoba-Jabonero, C., Sorribas, M., Guerrero-Rascado, J. L., Adame, J. A., Hernández, Y., Lyamani, H., Cachorro, V., Gil, M., Alados-Arboledas, L., Cuevas, E., and de la Morena, B.: Synergetic monitoring of Saharan dust plumes and potential impact on surface: a case study of dust transport from Canary Islands to Iberian Peninsula, Atmos. Chem. Phys., 11, 3067–3091, doi:10.5194/acp-11-3067-2011, 2011.

Draxler, R. R. and Rolph, G. D.: HYSPLIT (Hybrid Single-Particle Lagrangian Integrated Trajectory). Model access via NOAA ARL READY website http://ready.arl.noaa.gov/HYSPLIT.php (last access: May 2012), 2003.

Dubovik, O. and King, M. D.: A flexible inversion algorithm for retrieval of aerosol optical properties from sun and sky radiance measurements, J. Geophys. Res., 105, 20673–20696, 2000.

Dubovik, O., Holben, B., Eck, T. F., Smirnov, A., Kaufman, Y. J., King, M. D., Tanre, D., and Slutsker, I.: Variability of absorption and optical properties of key aerosol types observed in worldwide locations, J. Atmos. Sci., 59, 590–608, 2002.

Dubovik, O., Sinyuk, A., Lapyonok, T., Holben, B. N., Mischenko, M., Yang, P., Eck, T. F., Volten, H., Muñoz, O., Veihelmann, B., van der Zande, W. J., Leon, J. F., Sorokin, M., and Slutsker, I.: Application of spheroid models to account for aerosol particle nonsphericity in remote sensing of desert dust, J. Geophys. Res.-Atmos., 111, D11208, doi:10.1029/2005JD006619, 2006.

Eck, T. F., Holben, B. N., Reid, J. S., Dubovik, O., Smirnov, A., O'Neill, N. T., Slutsker, I., and Kinne, S.: Wavelength dependence of the optical depth of biomass burning, urban, and desert dust aerosols, J. Geophys. Res.-Atmos., 104, 31333–31349, 1999.

Eck, T. F., Holben, B. N., Ward, D. E., Dubovik, O., Reid, J. S., Smirnov, A., Mukelabai, M. M., Hsu, N. C., O'Neill, N. T., and Slutsker, I.: Characterization of the optical properties of biomass burning aerosols in Zambia during the 1997 ZIBBEE field campaign, J. Geophys. Res.-Atmos., 106, 3425–3448, doi:10.1029/2000jd900555, 2001.

Eck, T. F., Holben, B. N., Reid, J. S., O'Neill, N. T., Schafer, J. S., Dubovik, O., Smirnov, A., Yamasoe, M. A., and Artaxo, P.: High aerosol optical depth biomass burning events: A comparison of optical properties for different source regions, Geophys. Res. Lett., 30, 2035, doi:10.1029/2003gl017861, 2003a.

Eck, T. F., Holben, B. N., Ward, D. E., Mukelabai, M. M., Dubovik, O., Smirnov, A., Schafer, J. S., Hsu, N. C., Piketh, S. J., Queface, A., Le Roux, J., Swap, R. J., and Slutsker, I.: Variability of biomass burning aerosol optical characteristics in southern Africa during the SAFARI 2000 dry season campaign and a comparison of single scattering albedo estimates from radiometric measurements, J. Geophys. Res.-Atmos., 108, 8477, doi:10.1029/2003jd001606, 2003b.

Esposito, F., Serio, C., Pavese, G., Auriemma, G., and Satriano, C.: Measurements of nighttime atmospheric optical depth: Preliminary data from mountain site in southern Italy, J. Aerosol Sci., 29, 1213–1218, 1998.

Estelles, V., Martinez-Lozano, J. A., Utrillas, M. P., and Campanelli, M.: Columnar aerosol properties in Valencia (Spain) by ground-based Sun photometry, J. Geophys. Res.-Atmos., 112, D11201, doi:10.1029/2006jd008167, 2007.

Forster, P., Ramaswamy, V., Artaxo, P., Berntsen, T., Betts, R., Fahey, D. W., Haywood, J., Lean, J., Lowe, D. C., Myhre, G., Nganga, J., R. Prinn, Raga, G., Schulz, M., and Dorland, R. V.: Changes in Atmospheric Constituents and in Radiative Forcing, Climate Change 2007: The Physical Science Basis, in: Contribution of Working Group I to the Fourth Assessment Report of the Intergovernmental Panel on Climate Change, edited by: Solomon, S., Qin, D., Manning, M., Chen, Z., Marquis, M., Averyt, K. B., Tignor, M., and Miller, H. L., 2007.

García, O. E, Díaz, A. M., Exposito, F. J., Díaz, J. P., Redondas, A., and Sasaki, T.: Aerosol radiative forcing and forcing efficiency in the UVB for regions affected by Saharan and Asian mineral dust, J. Atmos. Sci., 66, 1033–1040, 2009.

Gobbi, G. P., Kaufman, Y. J., Koren, I., and Eck, T. F.: Classification of aerosol properties derived from AERONET direct sun data, Atmos. Chem. Phys., 7, 453–458, doi:10.5194/acp-7-453-2007, 2007.

Guerrero-Rascado, J. L., Olmo, F. J., Avilés-Rodríguez, I., Navas-Guzmán, F., Pérez-Ramírez, D., Lyamani, H., and Alados Arboledas, L.: Extreme Saharan dust event over the southern Iberian Peninsula in september 2007: active and passive remote sensing from surface and satellite, Atmos. Chem. Phys., 9, 8453–8469, doi:10.5194/acp-9-8453-2009, 2009.

Haywood, J. M. and Shine, K. P.: Multi-spectral calculations of the direct radiative forcing of tropospheric sulphate and soot aerosols using a column model, Q. J. Roy. Meteorol. Soc.-Part A, 123, 1907–1930, 1997.

Herber, A., Thomason, L. W., Gernandt, H., Leiterer, U., Nagel, D., Schulz, K. H., Kaptur, J., Albrecht, T., and Notholt, J.: Continuous day and night aerosol optical depth observations in the Arctic between 1991 and 1999, J. Geophys. Res.-Atmos., 107, 4097, doi:10.1029/2001jd000536, 2002.

Holben, B. N., Eck, T. F., Slutsker, I., Tanre, D., Buis, J. P., Setzer, A., Vermote, E., Reagan, J. A., Kaufman, Y. J., Nakajima, T., Lavenu, F., Jankowiak, I., and Smirnov, A.: AERONET – A federated instrument network and data archive for aerosol characterization, Remote Sens. Environ., 66, 1–16, 1998.

Kahn, R. A., Gaitley, B. J., Martonchik, J. V., Diner, D. J., Crean, K. A., and Holben, B.: Multiangle Imaging Spectroradiometer (MISR) global aerosol optical depth validation based on 2 years of coincident Aerosol Robotic Network (AERONET) observations, J. Geophys. Res.-Atmos., 110, D10s04, doi:10.1029/2004jd004706, 2005.

Kaufman, Y. J., Wald, A. E., Remer, L. A., Gao, B. C., Li, R. R., and Flynn, L.: The MODIS 2.1-mu m channel – Correlation with visible reflectance for use in remote sensing of aerosol, IEEE T. Geosci. Remote Sens., 35, 1286–1298, 1997.

Kaufman, Y. J., Tanre, D., and Boucher, O.: A satellite view of aerosols in the climate system, Nature, 419, 215–223, doi:10.1038/nature01091, 2002.

Kotchenruter, R. A., Hobbs, P. V., and Hegg, D. A.: Humidification factors for atmospheric aerosol off the mid-Atlantic coast of United States, J. Geophys. Res.-Atmos., 98, 2239–2252, 1999.

Leiterer, U., Naebert, A., Naebert, T., and Alekseeva, G.: A new star photometer developed for spectral aerosol optical thickness measurements in Lindenberg, Contributions to Atmospheric Physics, 68, 133–141, 1995.

Lyamani, H., Olmo, F. J., and Alados-Arboledas, L.: Saharan dust outbreak over southeastern Spain as detected by sun photometer, Atmos. Environ., 39, 7276–7284, doi:10.1016/j.atmosenv.2005.09.011, 2005.

Lyamani, H., Olmo, F. J., Alcantara, A., and Alados-Arboledas, L.: Atmospheric aerosols during the 2003 heat wave in southeastern Spain II: Microphysical columnar properties and radiative forcing, Atmos. Environ., 40, 6465–6476, doi:10.1016/j.atmosenv.2006.04.047, 2006a.

Lyamani, H., Olmo, F. J., Alcantara, A., and Alados-Arboledas, L.: Atmospheric aerosols during the 2003 heat wave in southeastern Spain I: Spectral optical depth, Atmos. Environ., 40, 6453–6464, doi:10.1016/j.atmosenv.2006.04.048, 2006b.

Lyamani, H., Olmo, F. J., and Alados-Arboledas, L.: Light scattering and absorption properties of aerosol particles in the urban environment of Granada, Spain, Atmos. Environ., 42, 2630–2642, 2008.

Lyamani, H., Olmo, F. J., and Alados-Arboledas, L.: Physical and optical properties of aerosols over an urban location in Spain: seasonal and diurnal variability, Atmos. Chem. Phys., 10, 239–254, doi:10.5194/acp-10-239-2010, 2010.

Lyamani, H., Olmo, F. J., Foyo, I., and Alados-Arboledas, L.: Black carbon aerosol over an urban area in south-eastern Spain: Changes detected after the 2008 economic crisis, Atmos. Environ., 45, 6423–6432, 2011.

Mazzola, M., Lanconelli, C., Lupi, A., Busetto, M., Vitale, V., and Tomasi, C.: Columnar aerosol optical properties in the Po Valley, Italy, from MFRSR data, J. Geophys. Res.-Atmos., 115, D17206, doi:10.1029/2009jd013310, 2010.

Meloni, D., di Sarra, G., Biavati, G., DeLuisi, J. J., Monteleone, F., Pace, G., Piacentino, S., and Sferlazzo, D. M.: Seasonal behaviour of Saharan dust events at the Mediterranean island of Lampedusa in the period 1999–2005, Atmos. Environ., 41, 3041–3056, 2007.

Millan, M. M., Salvador, R., and Matilla, E.: Photo-oxidant dynamics in the Mediterranean basin in summer: Results from European research projects, J. Geophys. Res.-Atmos., 102, 8811–8823, 1997.

Miller, K. A., Siscovick, D. S., Sheppard, L., Shepherd, K., Sullivan, J. H., Anderson, G. L., and Kaufman, J. D.: Long-term exposure to air pollution and incidence of cardiovascular events in women, New England Journal of Medicine, 356, 447–458, doi:10.1056/NEJMoa054409, 2007.

O'Neill, N. T., Eck, T. F., Holben, B. N., Smirnov, A., and Dubovik, O.: Bimodal size distribution influences on the variation of Angström derivates in spectral and optical depth space, J. Geophys. Res.-Atmos., 106, 9787–9806, 2001.

O'Neill, N. T., Eck, T. F., Smirnov, A., Holben, B. N., and Thulasiraman, S.: Spectral discrimination of coarse and fine mode optical depth, J. Geophys. Res.-Atmos., 108, 4559, doi:10.1029/2002jd002975, 2003.

Olmo, F. J., Quirantes, A., Alcántara, A., Lyamani, H., and Alados-Arboledas, L.: Preliminary results of a non-spherical aerosol method for retrieving of the atmospheric aerosol optical properties, J. Quant. Spectrosc. Ra. Transfer, 100, 305–314, 2006.

Olmo, F. J., Quirantes, A., Lara, V., Lyamani, H., and Alados-Arboledos, L.: Aerosol optical properties assesed by an inversion method using the solar principal plane for non-spherical particles, J. Quant. Spectrosc. Ra. Transfer, 109, 1504–1516, 2008.

Pace, G., di Sarra, A., Meloni, D., Piacentino, S., and Chamard, P.: Aerosol optical properties at Lampedusa (Central Mediter-

ranean). 1. Influence of transport and identification of different aerosol types, Atmos. Chem. Phys., 6, 697–713, doi:10.5194/acp-6-697-2006, 2006.

Pandolfi, M., Cusack, M., Alastuey, A., and Querol, X.: Variability of aerosol optical properties in the Western Mediterranean Basin, Atmos. Chem. Phys., 11, 8189–8203, doi:10.5194/acp-11-8189-2011, 2011.

Pappalardo, G., Wandinger, U., Mona, L., Hiebsch, A., Mattis, I., Amodeo, A., Ansmann, A., Seifert, P., Linné, H., Apituley, A., Alados-Arboledas, L., Balis, D., Chaikovsky, A., D' Amico, G., De Tomasi, F., Freudenthaler, V., Giannakaki, E., Giunta, A., Grigorv, I., Iarolori, M., Madonna, F., Mamouri, R.E., Nasti, L., Papayannis, A., Pietruczuk, A., Pujadas, M., Rizi, V., Rocadenbosch, F., Russo, F., Schnell, F., Spinelli, M., Wang, W., and Wiegner, M.: EARLINET correlative measurements for CALIPSO: First intercomparison, J. Geophys. Res.-Atmos., 115, D00H19, doi:10.1029/2009JD012147, 2009.

Pavese, G., De Tomasi, F., Calvello, M., Esposito, F., and Perrone, M. R.: Detection of Sahara dust intrusions during mixed advection patterns over south-east Italy: A case study, Atmos. Res., 92, 489–504, doi:10.1016/j.atmosres.2009.02.003, 2009.

Perez-Ramirez, D., Aceituno, J., Ruiz, B., Olmo, F. J., and Alados-Arboledas, L.: Development and calibration of a star photometer to measure the aerosol optical depth: Smoke observations at a high mountain site, Atmos. Environ., 42, 2733–2738, doi:10.1016/j.atmosenv.2007.06.009, 2008a.

Perez-Ramirez, D., Ruiz, B., Aceituno, J., Olmo, F. J., and Alados-Arboledas, L.: Application of Sun/star photometry to derive the aerosol optical depth, Int. J. Remote Sens., 29, 5113–5132, doi:10.1080/01431160802036425, 2008b.

Perez-Ramirez, D., Lyamani, H., Olmo, F. J., and Alados-Arboledas, L.: Improvements in star photometry for aerosol characterizations, J. Aerosol Sci., 42, 737–745, 2011.

Pérez-Ramírez, D., Navas-Guzman, F., Lyamani, H., Fernandez-Galvez, J., Olmo, F. J., and Alados-Arboledas, L.: Retrievals of precipitable water vapor using star photometry: assesment with Raman lidar and link to sun photometry, J. Geophys. Res., 117, D05202, doi:10.1029/2011JD016450, 2012a.

Pérez-Ramírez, D., Lyamani, H., Olmo, F. J., Whiteman, D. N., Navas-Guzmán, F., and Alados-Arboledas, L.: Cloud screening and quality control algorithm for star photometer data: assessment with lidar measurements and with all-sky images, Atmos. Meas. Tech., 5, 1585–1599, doi:10.5194/amt-5-1585-2012, 2012b.

Perrone, M. R., Santese, M., Tafuro, A. M., Holben, B., and Smirnov, A.: Aerosol load characterization over South-East Italy for one year of AERONET sun-photometer measurements, Atmos. Res., 75, 111–133, doi:10.1016/j.atmosres.2004.12.003, 2005.

Pope, C. A., Burnett, R. T., Thun, M. J., Calle, E. E., Krewski, D., Ito, K., and Thurston, G. D.: Lung cancer, cardiopulmonary mortality, and long-term exposure to fine particulate air pollution, JAMA-J. Am. Med. Assoc., 287, 1132–1141, doi:10.1001/jama.287.9.1132, 2002.

Prats, N., Cachorro, V. E., Sorribas, M., Mogo, S., Berjon, A., Toledano, C., de Frutos, A. M., de la Rosa, J., Laulainen, N., and de la Morena, B. A.: Columnar aerosol optical properties during "El Arenosillo 2004 summer campaign", Atmos. Environ., 42, 2643–2653, doi:10.1016/j.atmosenv.2007.07.041, 2008.

Querol, X., Pey, J., Pandolfi, M., Alastuey, A., Cusack, M., Perez, N., Moreno, T., Viana, M., Mihalopoulos, N., Kallos, G., and Kleanthous, S.: African dust contributions to mean ambient PM(10) mass-levels across the Mediterranean Basin, Atmos. Environ., 43, 4266–4277, doi:10.1016/j.atmosenv.2009.06.013, 2009.

Randriamiarisoa, H., Chazette, P., Couvert, P., Sanak, J., and Mégie, G.: Relative humidity impact on aerosol parameters in a Paris suburban area, Atmos. Chem. Phys., 6, 1389–1407, doi:10.5194/acp-6-1389-2006, 2006.

Raut, J.-C. and Chazette, P.: Retrieval of aerosol complex refractive index from a synergy between lidar, sunphotometer and in situ measurements during LISAIR experiment, Atmos. Chem. Phys., 7, 2797–2815, doi:10.5194/acp-7-2797-2007, 2007.

Reid, J. S., Hobbs, P. V., Ferek, R. J., Blake, D. R., Martins, J. V., Dunlap, M. R., and Liousse, C.: Physical, chemical, and optical properties of regional hazes dominated by smoke in Brazil, J. Geophys. Res.-Atmos., 103, 32059–32080, 1998.

Reid, J. S., Eck, T. F., Christopher, S. A., Hobbs, P. V., and Holben, B.: Use of the Angstrom exponent to estimate the variability of optical and physical properties of aging smoke particles in Brazil, J. Geophys. Res.-Atmos., 104, 27473–27489, doi:10.1029/1999jd900833, 1999.

Remer, L. A., Kaufman, Y. J., Tanre, D., Mattoo, S., Chu, D. A., Martins, J. V., Li, R. R., Ichoku, C., Levy, R. C., Kleidman, R. G., Eck, T. F., Vermote, E., and Holben, B. N.: The MODIS aerosol algorithm, products, and validation, J. Atmos. Sci., 62, 947–973, 2005.

Rodríguez, S., Querol, X., Alastuey, A., Kallos, G., and Kakaliagou, O.: Saharan dust contributions to PM10 and TSP levels in Southern and Eastern Spain, Atmos. Environ., 35, 2433–2447, doi:10.1016/s1352-2310(00)00496-9, 2001.

Rodríguez, S., Alastuey, A., Alonso-Pérez, S., Querol, X., Cuevas, E., Abreu-Afonso, J., Viana, M., Pérez, N., Pandolfi, M., and de la Rosa, J.: Transport of desert dust mixed with North African industrial pollutants in the subtropical Saharan Air Layer, Atmos. Chem. Phys., 11, 6663–6685, doi:10.5194/acp-11-6663-2011, 2011.

Sanchez, S. F., Aceituno, J., Thiele, U., Perez-Ramirez, D., and Alves, J.: The night sky at the Calar Alto observatory, Publ. Astron. Soc. Pac., 119, 1186–1200, doi:10.1086/522378, 2007.

Santese, M., De Tomasi, F., and Perrone, M. R.: Advection patterns and aerosol optical and microphysical properties by AERONET over south-east Italy in the central Mediterranean, Atmos. Chem. Phys., 8, 1881–1896, doi:10.5194/acp-8-1881-2008, 2008.

Sasano, Y., Browell, E. V., and Ismail, S.: Error caused by using a constant extinction/backscattering ratio in the lidar solution, Appl. Optics, 24, 3929–3932, 1985.

Schuster, G. L., Dubovik, O., and Holben, B. N.,: Angström exponent and bimodal aerosol size distributions, J. Geophys. Res., 111, D07207, doi:10.1029/2005JD006328, 2006.

Seinfeld, J. H. and Pandis, S. N.: Atmospheric chemistry and physics from air pollution to climate change John Wiley & Sons, 1998.

Smirnov A., Holben, B. N., Eck, T. F., Dubovik, O., and Slutsker, I.: Cloud screening and quality control algorithms for the AERONET data base, Remote Sens. Environ., 73, 337–349, 2000.

Titos, G., Foyo-Moreno, I., Lyamani, H., Querol, X., Alastuey, A., and Alados-Arboledas, L.: Optical properties and chemical composition of aerosol particles at an urban location: An estimation of the aerosol mass scattering and absorption efficiencies, J. Geophys. Res.-Atmos., 117, D04206, doi:10.1029/2011JD016671, 2012.

Toledano, C., Cachorro, V. E., de Frutos, A. M., Sorribas, M., Prats, N., and de la Morena, B.: Inventory of African desert dust events over the southwestern Iberian Peninsula in 2000–2005 with an AERONET Cimel Sun photometer, J. Geophys. Res.-Atmos., 112, D21201, doi:10.1029/2006JD008307, 2007a.

Toledano, C., Cachorro, V. E., Berjon, A., de Frutos, A. M., Sorribas, M., de la Morena, B. A., and Goloub, P.: Aerosol optical depth and Angstrom exponent climatology at El Arenosillo AERONET site (Huelva, Spain), Q. J. Roy. Meteorol. Soc., 133, 795–807, doi:10.1002/qj.54, 2007b.

Toledano, C., Cachorro, V. E., De Frutos, A. M., Torres, B., Berjón, A., Sorribas, M., and Stone, R. S.: Airmass Classification and Analysis of Aerosol Types at El Arenosillo (Spain), J. Appl. Meteorol. Climatol., 48, 962–981, 2009.

Valenzuela, A., Olmo, F. J., Lyamani, H., Antón, M., Quirantes, A., and Alados-Arboledas, L.: Analysis of the columnar radiative properties retrieved during African desert dust events over Granada (2005–2010) using principal plane sky radiances and spheroids retrieval procedure, Atmos. Res., 105, 292–301, doi:10.1016/j.atmosres.2011.11.005, 2012a.

Valenzuela, A., Olmo, F. J., Lyamani, H., Antón, M., Quirantes, A., and Alados-Arboledas, L.: Classification of aerosol radiative properties during African desert dust intrusions over southeastern Spain by sector origins and cluster analysis, J. Geophys. Res.-Atmos., 117, D06214, doi:10.1029/2011JD016885, 2012b.

Veselovskii, I., Whiteman, D., Kolgotin, A., Andrews, E., and Korenskii, M.: Demonstration of aerosol property profiling by multiwavelenght lidar under varying relative humidity conditions. J. Atmos. Ocean. Tech., 26, 1543–1557, doi:10.1175/2009JTECHA1254.1, 2009.

Welton, E. J., Campbell, J. R., Spinhirne, J. D., and Scott, V. S.: Global monitoring of clouds and aerosols using a network of micro'pulse lidar systems, Proc. SPIE Lidar remote sensing for industry and environmental monitoring, 4153, 151–158, 2001.